Enteroendocrine cells sense bacterial tryptophan catabolites to activate enteric and vagal neuronal pathways

Lihua Ye[1,2], Munhyung Bae[3], Chelsi D. Cassilly[3], Sairam, V. Jabba[4], Hsiu-Yi Lu[1], Jinhu Wang[5], John D. Thompson[6], Colin R. Lickwar[1,2], Kenneth D. Poss[6], Sven-Eric Jordt[4], Jon Clardy[3], Rodger A. Liddle[2,7], and John F. Rawls[1,2]

[1] Department of Molecular Genetics and Microbiology, Duke Microbiome Center, Duke University School of Medicine, Durham, NC, 27710

[2] Division of Gastroenterology, Department of Medicine, Duke University School of Medicine, Durham, NC, 27710

[3] Department of Biological Chemistry and Molecular Pharmacology, Harvard Medical School, Boston, MA, 02115

[4] Department of Anesthesiology, Duke University School of Medicine, Durham, NC, 27710

[5] Division of Cardiology, School of Medicine, Emory University, Atlanta, GA 30322

[6] Department of Cell Biology, Duke University School of Medicine, Durham, NC, 27710

[7] Department of Veterans Affairs, Durham, NC 27705

SUMMARY

The intestinal epithelium senses nutritional and microbial stimuli using epithelial sensory enteroendocrine cells (EECs). EECs can communicate nutritional information to the nervous system, but similar mechanisms for microbial information are unknown. Using *in vivo* real-time measurements of EEC and nervous system activity in zebrafish, we discovered that the bacteria *Edwardsiella tarda* specifically activates EECs through the receptor transient receptor potential ankyrin A1 (Trpa1) and increases intestinal motility in an EEC-dependent manner. Microbial, pharmacological, or optogenetic activation of Trpa1^{+}EECs directly stimulates vagal sensory ganglia and activates cholinergic enteric neurons through 5-HT. We identified a distinct subset of indole derivatives of tryptophan catabolites produced by *E. tarda* that potently activate zebrafish EEC Trpa1 signaling and also directly activate human and mouse Trpa1. These results establish a molecular pathway by which EECs regulate enteric and vagal neuronal pathways in response to specific microbial signals.

INTRODUCTION

The intestine harbors a complex microbial community that shapes intestinal physiology, modulates systemic metabolism, and regulates brain function. These effects on host biology are often evoked by distinct microbial stimuli including microbe-associated molecular patterns (MAMPs) and microbial metabolites derived from digested carbohydrates, proteins, lipids, and bile acids [1-3]. The intestinal epithelium is the primary interface that mediates this host-microbe communication [4]. The mechanisms by which the intestinal epithelium senses distinct microbial stimuli and transmits that information to the rest of the body remains incompletely understood.

The intestinal epithelium has evolved specialized enteroendocrine cells (EECs) that exhibit conserved sensory functions in insects, fish, and mammals [5-7]. Distributed along the entire digestive tract, EECs are activated by diverse luminal stimuli to secrete hormones or neuronal

transmitters in a calcium dependent manner [7]. Recent studies have shown that EECs form synaptic connections with sensory neurons [8, 9]. The connection between EECs and neurons forms a direct route for the intestinal epithelium to transmit nutrient sensory information to the brain [8]. EECs are classically known for their ability to sense nutrients [10] but whether they can be directly stimulated by microbes or microbially derived products is less clear. Limited examples include the observation that short chain fatty acids and branched chain fatty acids from microbial carbohydrate and amino acid catabolism activate EECs via G-protein coupled receptors [9, 11]. Indole, a microbial catabolite of the amino acid tryptophan, has also been reported to activate EECs, but the EEC receptor that mediates the effect remains unidentified [12]. With the growing understanding of gut microbiota and their metabolites, identifying the EEC receptors that recognize distinct microbial stimuli as well as the downstream pathways by which EECs transmit microbial stimuli to regulate local and systemic host physiology, have emerged as important goals.

The vertebrate intestine is innervated by the intrinsic enteric nervous system (ENS) and extrinsic neurons from autonomic nerves, including sensory nerve fibers from the nodose vagal ganglia and dorsal root ganglia in the spinal cord [13]. Both vagal and spinal sensory nerve fibers transmit visceral stimuli to the central nervous system and modulate a broad spectrum of brain functions [14]. A previous study demonstrated that stimulating EECs with the microbial metabolite isovalerate activates spinal sensory nerves through 5-hydroxytryptamine (5-HT) secretion [9]. Whether and how gut microbial stimuli modulate ENS or vagal sensory activity through EECs is still unknown.

EECs are known to express a broad diversity of receptors and channels to perceive and respond to environmental stimuli [7]. Transient receptor potential ankyrin 1 (Trpa1) is an excitatory calcium-permeable non-selective cation channel that can be activated by multiple chemical irritants and has important roles in pain sensation and neurologic inflammation [15, 16]. Many of the known Trpa1 agonists are chemicals derived from food spices or environmental pollution [17]. Whether microbial metabolites also activate Trpa1 is completely unknown.

Here, we show that Trpa1 is expressed in a subset of EECs that can be uniquely activated by gut microbes. Specifically, we identified a gram-negative bacterium, *Edwardsiella tarda* (*E. tarda*), that activates EECs in a Trpa1 dependent manner. Microbial, optochemical, or optogenetic activation of Trpa1+EECs activates vagal sensory ganglia and increases intestinal motility through direct signaling to enteric motor neurons. Importantly, we have identified a subset of tryptophan catabolites that are secreted from *E. tarda* and potently activate Trpa1, stimulate intestinal motility, and activate vagal neurons.

RESULTS

Edwardsiella tarda activates EECs through Trpa1

To identify stimuli that activate EECs in live animals, we developed a new transgenic zebrafish line that permits recording of EEC activity by expressing the calcium modulated photoactivatable ratiometric integrator (CaMPARI) protein in EECs under control of the *neurod1* promoter [6] (Fig. 1A, Fig. S1A-B). When exposed to 405nm light, CaMPARI protein in the presence of high levels of intracellular calcium ($[Ca^{2+}]_i$) undergoes permanent photoconversion (PC) from green to red fluorescence emission [18]. This EEC-CaMPARI system therefore enables imaging of the calcium activity history of intestinal EECs in the intact physiologic context of live free-swimming animals. We established an assay system in which *Tg(neurod1:CaMPARI)* zebrafish larvae at 6 days post-fertilization (dpf) are separated into groups and exposed to specific stimulants for a designated

period of time, followed by application of a brief 405nm light pulse (30s) to photoconvert CaMPARI (Fig. 1A). The recent history of EEC activity in response to the respective stimulus can then be estimated by measuring the ratio of red:green CaMPARI fluorescence in EECs (Fig. 1B, Fig. S1G-I). To test the validity of this EEC-CaMPARI system, we first stimulated larvae with different nutrient stimuli known to activate zebrafish EECs [6]. Exposure to only water as a vehicle control revealed an expected low basal red:green CaMPARI ratio (Fig. 1C, E-F). Following long-chain fatty acid stimulation with linoleate, a subpopulation of EECs displayed high red:green CaMPARI ratio (Fig. 1D, E-F). EECs with a high red:green CaMPARI ratio were classified as "activated EECs". The percentage of activated EECs significantly increased in response to chemical stimuli known to activate EECs, including linoleate, oleate, laurate, and glucose (Fig. 1F), but not in response to the short chain fatty acid butyrate (Fig. 1F) [6]. This new EEC-CaMPARI system therefore permits recording of EEC activity in live free-swimming zebrafish consistent with alternative assay systems that require animal immobilization [6].

We next applied the EEC-CaMPARI system to ask whether EECs acutely respond to live bacterial stimulation *in vivo*. We exposed *Tg(neurod1:CaMPARI)* zebrafish to individual bacterial strains for 20 mins, followed by photoconversion and imaging of CaMPARI fluorescence. For these experiments, we selected a panel of 11 bacterial strains including 3 model species (*Pseudomonas aeruginosa*, *Escherichia coli*, *Bacillus subtilis*), 7 commensal strains isolated from the zebrafish intestine [19, 20], and the pathogen *Edwardsiella tarda* FL6-60 (also called *E. piscicida* [21, 22]; Fig. 1K and Table S1). Within this panel, the only strain that induced a high red:green EEC-CaMPARI signal was *E. tarda* (Fig. 1G-K). To further confirm that *E. tarda* directly activated EECs, we applied an alternative reporter of EEC activity based on the $[Ca^{2+}]_i$-sensitive fluorescent protein Gcamp6f (*neurod1:Gcamp6f*) [6]. We found that the EEC-Gcamp6f fluorescence signal significantly increased 20 mins after *E. tarda* stimulation, consistent with the EEC-CaMPARI result described above (Fig. 1L, Fig. S1L-Q and Video 1). Although *E. tarda* has been reported to infect zebrafish [21, 23], we observed no overt pathogenesis in our experiments.

EECs express a variety of sensory receptors that can be activated by different environmental stimuli. To investigate the molecular mechanisms by which EECs perceive *E. tarda* stimulation, we isolated zebrafish EECs and performed RNA-seq analysis. To do so, we crossed two transgenic zebrafish lines, one that specifically expresses enhanced green fluorescent protein (EGFP) in all intestinal epithelial cells (*TgBAC(cldn15la:EGFP)*) [24] and a second that expresses red fluorescent protein (RFP) in EECs, pancreatic islets, and the central nervous system (CNS) (*Tg(neurod1:TagRFP)*) [25]. Transcript levels in FACS-sorted EECs (EGFP+; TagRFP+) were compared to all other intestinal epithelial cells (IECs) (EGFP+; TagRFP-) (Fig. 2A and Fig. S2A-B). We identified 192 zebrafish transcripts that were significantly enriched in EECs by DESeq2 using $P_{FDR}<0.05$ (Fig. 2B and Table S2). Gene Ontology (GO) term analysis revealed that those EEC-enriched zebrafish genes are enriched for processes like hormone secretion, chemical synaptic transmission and neuropeptide signaling (Fig. S2C). To identify gene homologs that are enriched in EECs in both zebrafish and mammals, we compared these 192 genes to published RNA-seq data from *Neurod1*+EECs from mouse duodenum and CHGA+ EECs from human jejunum [26]. Despite the evolutionary distance and differences in tissue origin, we found that 24% of zebrafish EEC-enriched gene homologs (46 out of 192) were shared among zebrafish, human, and mouse, and that 40% of zebrafish EEC-enriched genes (78 out of 192) were shared between zebrafish EECs and human jejunal EECs (Fig. 2C and Table S3). The genes with conserved EEC expression include those encoding specific hormones, transcription factors, G-protein coupled receptors, and ion channels that regulate membrane potential (Fig. 2C, Fig. S2D and Table S4).

Using published data from mouse intestinal epithelial single-cell RNA-seq data that revealed different EEC subtypes [27], we found that many of the signature genes in mouse enterochromaffin cells (EC), which are identified by their 5-HT synthesis, are enriched in zebrafish EECs (Fig. S3E). Among these conserved EEC-enriched genes, one of the genes with the highest expression in zebrafish EECs is transient receptor potential ankyrin 1 (Trpa1) (Fig. 2C and Fig. S3E).

The zebrafish genome encodes two *trpa1* paralogs, *trpa1a* and *trpa1b* [28]. RNA-seq data revealed that zebrafish EECs express *trpa1b* but not *trpa1a* (Fig. S3A-B). This finding was confirmed using RT-PCR from FACS-isolated EECs (Fig. S3C). Fluorescence imaging of *TgBAC(trpa1b:EGFP)* zebrafish [29] further revealed that *trpa1b* is expressed within the intestinal epithelium by a distinct subset of cells expressing the EEC marker *neurod1* (Fig. 2D-E). In addition, zebrafish EECs were activated by exposure to the Trpa1 agonist allyl isothiocyanate (AITC) (Fig. 2F, Fig. S2D and Video 2), whereas this response was inhibited by the Trpa1 antagonist HC030031 (Fig. S3G). AITC was unable to induce EEC activation in zebrafish homozygous for a *trpa1b* mutation but was able to induce EEC activation normally in *trpa1a* mutants [28] (Fig. 2F, Fig. S3E-F, H-I and Video 2). These data establish that *trpa1b*, but not *trpa1a*, is expressed by a subset of zebrafish EECs and is required for EEC activation by Trpa1 agonist AITC.

Trpa1 is a nociception receptor that is known to mediate pain sensation in nociceptive neurons [16]. A broad spectrum of chemical irritants, including many compounds that are derived from food spices, activate Trpa1 [17]. In addition to chemical irritants, certain bacterially derived components, including lipopolysaccharides (LPS) and hydrogen sulfide (H_2S), stimulated nociceptive neurons in a Trpa1-dependent manner [30]. Since the expression of classic microbial pattern recognition receptors is very low in zebrafish EECs (Fig. S3J-L), we tested if Trpa1 mediated *E. tarda*-induced EEC activation. We first treated wildtype (WT) *Tg(neurod1:CaMPARI)* fish with the Trpa1 antagonist HC030031, and observed that treatment with HC030031 significantly inhibited *E. tarda*'s ability to induce EEC activation (Fig. 2G-J). We similarly found that the ability of *E. tarda* to induce EEC activity in the EEC-CaMPARI model was blocked in *trpa1b* mutant zebrafish (Fig. 2K-N). In accord, experiments in *Tg(neurod1:Gcamp6f)* zebrafish confirmed that *Gcamp6f* fluorescence increased in EECs in response to *E. tarda* stimulation in WT, but not *trpa1b* mutant zebrafish (Fig. 2O-R). Therefore live *E. tarda* bacteria stimulate EECs in a Trpa1-dependent manner, suggesting that EEC Trpa1 signaling may play an important role in mediating microbe-host interactions.

EEC Trpa1 signaling is important to maintain microbial homeostasis by regulating intestinal motility

To determine how *E. tarda*-induced Trpa1 signaling in EECs affects the host, we exposed WT and *trpa1b*$^{-/-}$ zebrafish larvae to an *E. tarda* strain that expresses the mCherry fluorescent marker. When reared under conventional conditions in the absence of *E. tarda*, we observed no significant difference in the abundance of culturable gut microbes between *trpa1b*$^{+/+}$ and *trpa1b*$^{-/-}$ zebrafish (Fig. S4A-B). However, upon infection with *E. tarda*, there was significant accumulation of *E. tarda* mCherry^{+} bacteria in the intestinal lumen in *trpa1b*$^{-/-}$ but not *trpa1b*$^{+/+}$ zebrafish larvae (Fig. 3A-C). This accumulation could be observed by either quantifying *E. tarda* mCherry fluorescence (Fig. 3D) or counting *E. tarda* colony forming units (CFU) from dissected infected *trpa1b*$^{+/+}$ and *trpa1b*$^{-/-}$ zebrafish digestive tracts (Fig. 3E). This suggests that Trpa1 signaling may act as a host defense mechanism to facilitate clearance of enteric pathogens like *E. tarda*.

In addition to EECs, Trpa1 is also expressed in mesenchymal cells such as myoblasts within the intestine (Fig.2D-E and Fig. S6O) and nociceptive sensory neurons [31, 32]. To investigate whether the phenotype we observed above is specifically mediated by EECs, we generated new a Cre-*loxP* transgenic system that permits specific ablation of EECs (Fig. 3F). This system consists of two new transgene alleles - one expressing Cre recombinase from the *neurod1* promoter (in EECs, CNS, and islets) and a second expressing the diphtheria toxin (DTA) in *gata5*$^{+}$ cells (in EECs, other IECs, heart, and perhaps other cell types) only in the presence of Cre (Fig. 3F). As the only cells known to co-express *neurod1* and *gata5* in the zebrafish larvae, EECs are ablated whereas non-EEC cell populations, including islets and the CNS, remain unaffected (Fig. 3G). A small percentage of EECs remained in the distal intestine presumably due to the low level of *gata5* expression in that region (Fig. S4C). Quantitative RT-PCR and immunofluorescence results confirmed a reduction of EEC hormones but not non-EEC marker genes (Fig. S4F). Establishing this EEC ablation system allowed us to define the specific role of EECs in mediating *E. tarda*-host interaction. As with *trpa1b*$^{-/-}$ zebrafish, we did not detect significant differences in gut microbial abundance between unxposed WT and EEC-ablated zebrafish (Fig. S4G). However, in response to *E. tarda* exposure, a significantly higher amount of *E. tarda* mCherry accumulated in EEC-ablated zebrafish compared to WT sibling controls (Fig. 3H and Fig. S4H-I). Together, these data establish that EEC Trpa1 signaling maintains gut microbial homeostasis by facilitating host clearance of enteric pathogens like *E. tarda*.

To understand the mechanisms by which EEC Trpa1 regulates gut microbial homeostasis, we used an opto-pharmacological approach that permits the temporal control of EEC Trpa1 activation through UV light exposure (Fig. 4A). We pretreated zebrafish with Optovin, a chemical compound that specifically activates Trpa1 only in the presence of UV light [33] (Fig. S5A). To specifically activate Trpa1 in EECs, we mounted zebrafish larvae pretreated with Optovin and restrict UV light exposure specifically to the intestinal epithelium using a confocal laser (Fig. S5A). UV light activation significantly increased $[Ca^{2+}]_i$ in a subpopulation of EECs in WT larvae, as measured by Gcamp6f fluorescence (Fig. S5B-D, Video 3). The same UV light exposure in *trpa1b*$^{-/-}$ larvae pretreated with Optovin did not increase EEC $[Ca^{2+}]_i$ (Fig. 4B-C), indicating that the EEC activation induced by Optovin-UV was dependent on Trpa1. Next, we used this approach to examine the effect of EEC Trpa1 activation on intestinal motility. Trpa1 activation in EECs via UV light application in WT larvae produced a propulsive movement of the intestine from anterior to posterior, and the velocity of intestinal motility increased accordingly (Fig. 4D-F, Fig. S5E-G and Video 4). In contrast, Optovin treatment and UV activation failed to induce intestinal motility in EEC-ablated zebrafish larvae (Fig. 4D-F and Video 5). These results indicate that intestinal motility triggered by Trpa1 activation is dependent on EECs. To further test if signaling from Trpa1^{+}EECs is sufficient to activate intestinal motility, we developed a new optogenetic system in which a mCherry tagged Channelrhodopsin (ChR2-mCherry) is expressed in EECs from the *neurod1* promoter (Fig. 4G-H). Blue light activation of ChR2 causes cation influx and plasma membrane depolarization; $[Ca^{2+}]_i$ then increases through the activation of voltage-dependent calcium channels [34], that are abundantly expressed in zebrafish EECs (Fig. 4I-J and Video 6). This new tool permits selective activation of the ChR2-mCherry^{+} EECs using a confocal laser, without affecting the activity of nearby EECs (see Method section and Fig. S5H-I). We therefore used *Tg(neurod1:Gal4); Tg(UAS:ChR2-mCherry); TgBAC(trpa1b:EGFP)* larvae to selectively activate ChR2-mCherry expressing EECs that are either *trpa1b*+ or *trpa1b*-. We found that activation of *trpa1b*+ EECs but not *trpa1b*- EECs consistently increased intestinal motility (Fig. 4K-L, Fig. S5H-K and Video 7), again indicating a unique role for Trpa1+EECs in regulating

intestinal motility. Finally, we tested whether microbial activation of Trpa1 signaling in EECs also increased intestinal motility. Using microgavage to specifically deliver live *E. tarda* bacteria into the intestinal lumen [35], we found that *E. tarda* gavage significantly promoted intestinal peristalsis and motility when compared to PBS-gavaged controls (Fig. 4M-O and Video 8). These experiments together establish that activation of Trpa1 in EECs directly stimulates intestinal motility, and provide a potential physiologic mechanism underlying Trpa1-dependent clearance of *E. tarda* from the intestinal lumen.

EEC Trpa1 signaling promotes intestinal motility by activating excitatory enteric motor neurons

To test the role of the ENS in Trpa1-activated intestinal motility, we used zebrafish that lack an ENS due to mutation of the *ret* gene, a growth factor receptor required for migration and differentiation of neural crest progenitors into developing ENS structures [36]. Immunofluorescence demonstrated that *ret*$^{-/-}$ zebrafish lack all identifiable enteric nerves (the enteric nerves are marked by *NBT* transgenes, Fig. 5B and Fig. S6A-B), whereas EECs remain intact (the EECs are marked by *neurod1* transgenes, Fig. 5B) and responsive to Trpa1 agonist AITC stimulation (Fig. S6C-F). Using the Optovin-UV system (Fig. 5A), we observed that EEC Trpa1 activation increased intestinal motility in control (*ret*$^{+/+}$ or *ret*$^{+/-}$) but not *ret*$^{-/-}$ zebrafish (Fig. 5C-D and Fig. S6G-H). To further test whether the ENS mediates the intestinal motility induced by EEC Trpa1 activation, we used a second zebrafish mutant that lacks an ENS due to mutation of the transcription factor gene *sox10* [37]. Similar to *ret*$^{-/-}$ zebrafish larvae, *sox10*$^{-/-}$ zebrafish larvae lack an ENS but the EECs remain intact (Fig. S7I-L). Consistent with our results from *ret*$^{-/-}$ animals, activating EEC-Trpa1 signaling also failed to increase intestinal motility in *sox10*$^{-/-}$ zebrafish larvae (Fig. S7M-N). Together these data suggest that Trpa1+ EECs do not signal directly to enteric smooth muscle to promote intestinal motility, but instead signal to the ENS.

The ENS is a complex network composed of many different neuronal subtypes. Among these subtypes, cholinergic neurons secrete the excitatory neurotransmitter acetylcholine to stimulate other enteric neurons or smooth muscle [38, 39]. The cholinergic neurons are essential for normal intestinal motility [40]. One of the key enzymes for the synthesis of acetylcholine in the ENS is choline acetyltransferase (Chat) [41]. Using *TgBAC(chata:Gal4); Tg(UAS:NTR-mCherry)* transgenic zebrafish, we were able to visualize the cholinergic excitatory enteric motor neurons in the zebrafish intestine (Fig. 5E and Fig. S6R). Analysis of the secretory cell marker 2F11 in *TgBAC(chata:Gal4); Tg(UAS:NTR-mcherry)* animals revealed a subpopulation of EECs that directly contact *chata*+ enteric motor nerve endings (Fig. 5F, Fig. S7E-G and Video 9). Interestingly, those EECs that directly contact *chata*+ enteric motor neurons include some Trpa1+EECs (Fig. 5G-H). Previous mouse studies demonstrated that some EECs possess neuropods that form synaptic connections with sensory neurons [8, 9, 42]. We found that zebrafish EECs also possess neuropods marked by the presynaptic marker SV2 (Fig. S7A-C). The enrichment of presynaptic vesicle protein genes in zebrafish EECs was further confirmed by our zebrafish EEC RNA-seq data (Fig. S7H and Table S2). Similar to mammalian EECs, zebrafish EEC neuropods also contain abundant mitochondria (Fig. S7D) [43]. Therefore zebrafish EECs may have an evolutionarily conserved function to signal to neurons, as seen in mammals.

The direct contact of Trpa1+EECs with *chata*+ neurons suggested a direct signal to cholinergic enteric neurons. To investigate whether activation of Trpa1+EECs stimulates *chata*+ enteric neurons, we employed *TgBAC(chata:Gal4); Tg(UAS:Gcamp6s)* zebrafish, which permit recording of *in vivo* calcium activity in *chata*+ neurons (Fig. 5I-J). Upon Trpa1+EEC activation, Gcamp6s

fluorescence increased in *chata*+ enteric motor neurons (Fig. 5K,L and Video 10). Immunofluorescence results indicated that Trpa1 is not expressed in *chata*+ enteric motor neurons or in any other ENS cell type (Fig. S6O-S). This result indicated that *chata*+ enteric motor neurons cannot be directly activated by optic Trpa1 stimulation, but are instead activated via stimulation by Trpa1+ EECs. Previous mouse studies demonstrated that *Trpa1* mRNA is highly enriched in 5-HT-secreting EC cells [44]. Immunofluorescence staining for 5-HT indicated that, similar to mice, 5-HT expression in the zebrafish intestinal epithelium is also highly enriched in Trpa1+EECs (Fig. 5M). 5-HT in EECs is synthesized from tryptophan via Tryptophan hydroxylase 1 (Tph1) [45]. Zebrafish possess two *Tph1* paralogs, *tph1a* and *tph1b [46]*, but only *tph1b* is expressed in zebrafish EECs (Fig. S7L). The expression of *tph1b* in Trpa1+EECs was also confirmed by crossing a new *Tg(tph1b:mCherry-NTR)* transgenic line to *TgBAC(trpa1b:EGFP)* zebrafish (Fig. 5N and Fig. S7J-N). To investigate whether 5-HT mediates EEC Trpa1-induced intestinal motility, we tested whether a similar response was present in *tph1b*$^{+/+}$ and *tph1b*$^{-/-}$ zebrafish larvae [47] using the Optovin-UV platform. Under baseline conditions, we did not observe a significant difference in intestinal motility between *tph1b*$^{+/+}$ and *tph1b*$^{-/-}$ zebrafish (Fig. S7O). However, in response to UV stimulated EEC Trpa1 activation, intestinal motility was significantly reduced in *tph1b*$^{-/-}$ compared to *tph1b*$^{+/+}$ zebrafish (Fig. 5O). These findings suggest a working model in which Trpa1+EECs signal to excitatory cholinergic enteric motor neurons through 5-HT, which in turn stimulates intestinal motor activity.

Chemical and microbial stimulation of EEC Trpa1 signaling activate vagal sensory ganglia

The intestine is innervated by both intrinsic ENS and extrinsic sensory nerves from the brain and spinal cord [14]. The vagus nerve travels from the intestine to the brainstem and conveys visceral information to the CNS. The vagal sensory nerve bodies reside in the nodose ganglia [14] (Fig. 6A), however it is unknown if the zebrafish vagal sensory system innervates the intestine. The zebrafish vagal sensory ganglia can be labelled using *TgBAC(neurod1:EGFP)* or immuofluoresence staining of the neuronal marker acetylated α Tubulin (Ac-αTub) (Fig. 6B). Using lightsheet confocal imaging, we established that the vagal ganglia in zebrafish extends projections that innervate the intestine (Fig. 6B-C and Fig. S8A-B). In the intestinal area, we found a subpopulation of EECs in direct contact with vagal sensory nerve fibers (Fig. 6D). Using the *Tg(neurod1:cre); Tg(β-act2:Brainbow)* transgenic zebrafish system [48] (vagal-brainbow), in which individual vagal ganglion cells are labeled with different fluorescent colors through Cre recombination [49] (Fig. S8C), we revealed that the zebrafish vagal sensory ganglia cells also directly project to the vagal sensory region in the hindbrain (Fig. 6E-F). Using this vagal-brainbow system, we found vagal sensory nerves that are labelled by Cre recombination in both proximal and distal intestine (Fig. S8D-G). To further visualize the vagal sensory network in zebrafish, we used *Tg(isl1:EGFP)* zebrafish in which EGFP is expressed in vagal sensory ganglia but not in EECs or the ENS (Fig. 6G and Fig. S8H-J). Our data revealed that after leaving the vagal sensory ganglia, the vagus nerve travels along the esophagus and enters the intestine in the region between the pancreas and the liver (Fig. 6G and Fig. S8J). Direct contact of EECs and the vagus nerve can also be observed in *Tg(isl1:EGFP); Tg(neurod1:TagRFP)* zebrafish (Fig. 6H). These data demonstrate the existence of a vagal network in the zebrafish intestine.

We next investigated whether this vagal network is activated in response to enteric microbial stimulation with *E. tarda*. We gavaged *Tg(neurod1:Gcamp6f); Tg(neurod1:TagRFP)* zebrafish larvae with either PBS or live *E. tarda* bacteria. We found that 30 min after enteric stimulation with Trpa1 agonist AITC or *E. tarda*, but not after PBS vehicle stimulation, Gcamp6f fluorescence

intensity significantly increased in a subset of vagal sensory neurons (Fig. 6I-K, Fig. S8K-L and Video 11). This result indicated that acute enteric chemical or microbial stimulation directly activated vagal sensory neurons. To further investigate whether the vagal activation induced by enteric *E. tarda* was mediated by Trpa1+EECs, we used a published method that labels active zebrafish neurons through pERK immunofluorescence staining [50] to measure vagal activity. Delivering AITC to the zebrafish intestine by microgavage [35] increased the number of pERK+ vagal cells compared to PBS treatment (Fig. 6L-N, R). AITC-induced vagal activation was abrogated in the absence of EECs (Fig. 6N, R), indicating that Trpa1 signaling in the intestine increases vagal sensory activity in an EEC-dependent manner. Next, we gavaged live *E. tarda* bacteria into both WT and EEC-ablated zebrafish. Similar to Trpa1 chemical agonist stimulation, *E. tarda* gavage increased the number of activated pERK+ vagal sensory neurons in WT zebrafish (Fig. 6O-Q, S) but not in EEC ablated zebrafish (Fig. 6Q, S). Furthermore, the vagal activation induced by enteric *E. tarda* was dependent on Trpa,1 as pERK+ vagal cell number was significantly reduced in *E. tarda* treated *trpa1b*$^{-/-}$ zebrafish (Fig. 6T). Together, these results reveal that chemical or microbial stimuli in the intestine can stimulate Trpa1+ EECs, which then signal to the vagal sensory ganglia.

Tryptophan catabolites secreted from *E. tarda* activate the EEC Trpa1 gut-brain pathway

In order to identify the molecular mechanism by which *E. tarda* activates Trpa1 in EECs, we examined the effects of live and killed *E. tarda* cells and cell-free supernatant (CFS) from *E. tarda* cultures on EEC calcium activity (Fig. 7A). Formalin-killed or heat-killed *E. tarda* cells failed to stimulate EECs, however, CFS, at levels comparable to live *E. tarda* cells, stimulated EECs (Fig. 7A-B). The ability of *E. tarda* CFS to activate EECs was diminished in *trpa1b* mutant zebrafish (Fig. 7C), suggesting that a factor secreted from *E. tarda* has the ability to directly activate Trpa1 in EECs. We noticed that some known ligands for Trpa1 have structural similarities to bacterial catabolites of the amino acid tryptophan. HPLC-MS analysis revealed that *E. tarda* CFS is enriched for several indole ring-containing tryptophan catabolites (Fig. 7D and Fig. S9A-D), three of the most abundant being indole, tryptophol (IEt), and indole-3-carboxyaldhyde (IAld) (Fig. 7D and Fig. S9A-D). Several zebrafish commensal bacteria produce indole when cultured in rich medium; however, their ability to produce and secrete indole was significantly reduced when cultured in GZM (gnotobiotic zebrafish media) water in which our zebrafish experiments are conducted (Fig. S9E). In contrast to the other strains tested, *E. tarda* uniquely retained a high level of indole production and secretion when cultured in GZM water (Fig. S9E).

Bacteria can convert tryptophan, an essential amino acid in animals, into various catabolites such as indole and IAld that are not produced by host [51]. Previous studies suggested that several bacterial tryptophan catabolites activate the ligand-activated transcription factors aryl hydrocarbon receptor (Ahr) and pregnane X receptor (Pxr) to modulate gut microbial-immune homeostasis [51]. However, it remains unknown what other signal transduction mechanisms host animals might use to acutely sense and respond to tryptophan catabolites that are abundantly secreted by gut microbes. To test if *E. tarda* tryptophan catabolites activate EECs, we stimulated zebrafish larvae with those different catabolites and measured EEC activity. Indole and IAld, but not other tested tryptophan catabolites, strongly activated zebrafish EECs in a *trpa1b*-dependent manner (Fig. 7E-H and Video 12). Indole and IAld also activated the human TRPA1 receptor transfected into HEK cells (Fig. 7I-J and Fig. S9F). Both indole and IAld exhibited full TRPA1 agonist activity with an efficiency comparable to cinnamaldehyde (CAD), a well characterized TRPA1 activator (Fig. 7I-J and Fig. S9F) [52]. Both indole and IAld also activated mouse Trpa1,

but in a less potent manner (Fig. S9I-J). Both indole- and IAld-induced human and mouse Trpa1 activation were blocked by the TRPA1 inhibitor A967079 (Fig. 7K and Fig. S9G-H, J). These results establish that indole and IAld that are derived from microbial tryptophan catabolism are novel and evolutionarily-conserved agonists of vertebrate TRPA1 receptors.

Finally, we investigated whether indole and IAld can mimic live *E. tarda* bacterial stimulation and activate a similar gut-brain pathway through EEC Trpa1 signaling. Stimulating zebrafish larvae with indole directly induced an increase in intestinal motility (Fig. S9L-N). Using *Tg(neurod1:Gcamp6f);Tg(neurod1:TagRFP)* transgenic zebrafish in which vagal calcium levels can be recorded *in vivo*, we further tested whether indole or IAld activated zebrafish vagal sensory neurons. Enteric delivery of indole or IAld through microgavage significantly increased Gcamp6f fluorescence intensity in a subset of vagal sensory neurons (Fig. 7L-Q). This vagal sensory neuron activation induced by enteric indole stimulation was abrogated when a similar microgavage was performed in zebrafish larvae lacking EECs (Fig. 7L-Q). Together these data indicate that specific tryptophan catabolites produced by *E. tarda* and other bacteria directly activate Trpa1 on EECs which leads to activation of vagal sensory neurons.

DISCUSSION

Trpa1+EECs are frontline intestinal sensors

To monitor the complex and dynamic chemical and microbial environment within the intestinal lumen, animals evolved specialized sensory cells in the intestinal epithelium known as EECs [7]. EECs are distinguished from other intestinal epithelial cells by their remarkable ability to respond to a wide range of nutrients and other chemicals and to secrete a variety of peptide hormones and neurotransmitters. Recent studies suggest that mammalian EECs display complex heterogeneity [53]. A unique EEC subtype defined in mammals is the enterochromaffin cell (EC) which produces the neurotransmitter 5-HT [54]. A subset of zebrafish EECs are also known to express 5-HT [55]. In the current study, we identified a Trpa1 expressing EEC subtype that uniquely responds to specific microbial stimulation. We also found that zebrafish Trpa1^{+}EECs include the majority of EECs that express 5-HT, revealing similarity between zebrafish Trpa1^{+}EECs and mammalian ECs. In accord, mammalian EC have also been shown to express Trpa1 [9]. Our study provides further evidence that Trpa1^{+}EECs respond to chemical and microbial stimuli and inform both the ENS and the vagal sensory nervous system. Thus, Trpa1^{+}EECs appear to be uniquely positioned to protect the organism from harmful chemical and microbial stimuli by regulating GI motility and perhaps sending signals to the brain.

Microbially derived tryptophan catabolites interact with the host through Trpa1

Trpa1 is a primary nociceptor involved in pain sensation and neuroinflammation. Trpa1 can be activated by several environmental chemical irritants and inflammatory mediators [56], however, it is not known if and how Trpa1 might be activated by microbes. Tryptophan is an essential amino acid that is released in the intestinal lumen by dietary protein digestion or microbial synthesis. It is well known that gut microbes can catabolize tryptophan to produce a variety of metabolites, among which indole was the first discovered and often the most abundant [57]. The concentration of indole in fecal samples of healthy adult humans can reach 6.5mM [58]. These tryptophan-derived metabolites secreted by gut bacteria can act as interspecies and interkingdom signaling molecules. For example, among bacteria, tryptophan catabolites regulate microbial virulence gene expression, biofilm production, stress response and act as quorum sensing molecules [59, 60]. Blocking indole production in *E. tarda* reduces LPS production and antibiotic resistance [61],

suggesting a potential role for tryptophan catabolism in *E. tarda* pathogenesis. *E. tarda* did not cause overt pathogenesis in our enteric exposure experiments here, but its ability to produce high levels of indole and IAld allowed us to identify them as potent EEC activators. The sufficiency of indole and IAld to activate EECs and neuronal responses predicts that other pathogenic and commensal bacteria that produce these catabolites could induce similar host responses. Microbially-derived tryptophan catabolites have been also shown to act on the host in other contexts. Some microbially-derived tryptophan catabolites including indole and IAld may regulate immune homeostasis and intestinal barrier function through ligand binding to the transcription factors, aryl hydrocarbon receptor (Ahr) and pregnane X receptor (Pxr/Nr1i2) [62, 63]. One of the microbial tryptophan catabolites, tryptamine, activates epithelial 5-HT_4R and increases anion-dependent fluid secretion in the proximal mouse colon [64]. Whether other host receptors can recognize microbially derived tryptophan catabolites is unknown.

Here, we present evidence that bacteria-derived tryptophan catabolites activate Trpa1 in zebrafish, human, and mouse. A previous study suggested that indole also activates the yeast TRP channel homolog TRPY1 [65]. This together with our findings point to an ancient role for TRP channels in microbial metabolite sensing. In the mammalian small intestine, Trpa1 is predominantly expressed in EECs that synthesize 5-HT from tryptophan [44]. Our results indicate that intestinal colonization by bacteria that produce high levels of tryptophan catabolites (e.g., *E. tarda*) leads to detection of those catabolites by Trpa1+EECs leading to purging of those bacteria by increased intestinal motility. It is notable that this Trpa1+EEC population responsible for sensing tryptophan catabolites is also responsible for conversion of tryptophan into 5-HT. It is also interesting that the only other microbial metabolite previously shown to activate 5HT+Trpa1+EECs is isovalerate, a bacterial catabolite of the essential amino acid leucine [9]. This raises the intriguing possibility that the 5-HT producing Trpa1+EECs act as host sensors for bacterial catabolism of essential amino acids, which could provide the host with information about microbiota density, composition, or consumption of essential nutrients. We showed here that indole activation of Trpa1+EECs leads to an acute increase in intestinal motility that helps clear the bacterium from the host, but we speculate that this pathway likely regulates additional host physiologic responses. In addition to modulating the local GI environment, the microbially derived tryptophan catabolites can be absorbed into the circulation where they could activate Trpa1 in nociceptive nerves and the central nervous system [66]. Overactivation of Trpa1 signaling by microbial tryptophan catabolites outside of the intestinal epithelium may therefore contribute to the development of chronic pain or neurologic inflammation in the host.

Gut microbiota-EEC-ENS communication

Nerve fibers do not penetrate the gut epithelium therefore, sensation is believed to be a transepithelial phenomenon as the host senses gut contents through the relay of information from EECs to the ENS [67]. Using an *in vitro* preparation of mucosa–submucosa, it was shown that mechanical or electrical stimulation of mucosa activates submucosal neuronal ganglia, which was blocked by a 5-HT_1R antagonist [38]. This suggests that 5-HT released from EC cells stimulates intrinsic primary afferent neurons (IPANs) which then activate secondary neurons [67]. IPANs are primary sensors in the ENS that receive signals from the intestinal epithelium and communicate to other ENS neurons [68]. The morphologically identifiable junction between ECs and IPANs has not been identified, and it was believed that 5-HT released from EC acts on enteric nerves through a diffuse paracrine mechanism [67]. However, recent studies demonstrated that some EECs actually synapse with extrinsic sensory nerves [9, 42]. Whether similar physical connections exist

between EECs and the ENS is still unclear. Here, we demonstrated that EECs form a direct connection with cholinergic enteric neurons (*chata*+ neurons) in zebrafish. We also provided *in vivo* evidence that stimulating Trpa1^{+}EECs directly activated these cholinergic enteric neurons. Trpa1+EEC-coupled cholinergic neurons are likely to be either IPANs [69] or excitatory motor neurons that directly act on the intestinal smooth muscle [38, 70]. The direct communication between EECs and cholinergic excitatory neurons provides a mechanism whereby the intestine could quickly increase intestinal motility to expel the noxious stimuli and thereby protect the host organism.

90% of 5-HT in the intestine is produced by EC cells, and therefore, EC cell 5-HT secretion was thought to be important in regulating intestinal motility [54]. This hypothesis, however, was challenged by recent findings that depletion of EC 5-HT production in *Tph1*$^{-/-}$ mice had only minor effects on gastric emptying, intestinal transit, and colonic motility [45]. Therefore, the physiological role of EC 5-HT production and secretion remains unclear. Here, using *tph1b*$^{-/-}$ zebrafish, we present data suggesting that even though EEC 5-HT production does not alter normal intestinal motility, the absence of EEC 5-HT production significantly reduced the increased motility induced by Trpa1 activation. This indicates that EEC 5-HT signaling may be necessary for the coping response to chemical or microbial irritant stimulation [44, 71].

Gut microbiota are believed to be important for regulating GI motility. Mice raised under germ-free conditions display lower propulsive efficiency of contractions and abnormal colonic motility [72]. It has also been shown that the introduction of specific microbes can directly affect GI motility [73]. The association between gut microbiota and GI motility is also evident in human diseases such as irritable bowel syndrome (IBS). IBS patients usually display alterations in GI motility without intestinal inflammation and many patients with diarrhea-dominant IBS developed their symptoms after an acute enteric bacterial infection (e.g., post-infectious IBS) [74]. The high prevalence of small intestinal bacterial overgrowth (SIBO) in IBS patients has been confirmed in many clinical studies [74]. The mechanisms underlying gut microbiota-induced GI motility and the development of pathological conditions like IBS are unclear. Here, we provide evidence that a specific gut bacterium and its secreted tryptophan catabolites directly stimulate intestinal motility by activating EEC-ENS signaling. Indole, IAld and other tryptophan catabolites are produced by a wide range of bacteria, so we expect our results to be applicable to other bacteria and their host interactions. These findings offer new possibilities for therapeutic treatment strategies for gut microbiota associated GI disorders, by targeting microbial tryptophan catabolism pathways, microbial or host degradation of those catabolites, or targeting EEC microbial sensing and EEC-ENS signaling pathways.

Gut microbiota-EEC-CNS communication

A subpopulation of EECs possesses neuropods that directly synapse with neurons [8, 9, 43]. Using optogenetic and vagal electric signal recording in mice, it was demonstrated that EECs sense sugar and convey an electrical signal to vagal neurons through a direct EEC-vagal connection [8]. It has also been reported that ECs communicate with 3-HT$_3$R neurons, and that ECs transduce microbial metabolite and chemical irritant signals to spinal afferent nerves in mice [9]. Here, we show that similar to mammalian EECs, zebrafish EECs are highly enriched in presynaptic gene transcripts, as revealed by our zebrafish EEC RNA-seq. The EECs from larvae and adult zebrafish also display similar “neuropod” structures that form direct connections with cholinergic enteric neurons and the vagus nerve. Zebrafish neuropods are also enriched in presynaptic vesicles and mitochondria, key features previously identified in mice [43]. In zebrafish,

Trpa1^{+}EEC stimulation is directly coupled to the activation of enteric and vagal sensory neurons, suggesting that the EEC-neuronal connection and route of communication are conserved between fish and mammals.

The vagus nerve is the primary sensory pathway by which visceral information is transmitted to the CNS. Recent evidence suggests that the vagus nerve may play a role in communicating gut microbial information to the brain [75-77]. For example, the beneficial effects of *Bifidobacterium longum* and *Lactobacillus rhamnosus* in neurogenesis and behavior were abolished following vagotomy [78, 79]. However, direct evidence for whether and how vagal sensory neurons perceive and respond to gut bacteria has been lacking. Our results demonstrate that both live *E. tarda* and *E. tarda*-derived tryptophan catabolites activate vagal sensory ganglia through EEC Trpa1 signaling. Previous findings have shown that EC cells transmit microbial metabolite and chemical irritant stimuli to pelvic fibers from the spinal cord dorsal root ganglion [9]. Our findings here demonstrate that, in addition to spinal sensory nerves, EEC-vagal signaling is an important pathway for transmitting specific gut microbial signals to the CNS. The vagal ganglia project directly onto the hindbrain, and that vagal-hindbrain pathway has key roles in appetite and metabolic regulation [80-83]. Our findings raise the possibility that certain tryptophan catabolites, including indole, may directly impact these processes as well as emotional behavior and cognitive function [84]. If so, this pathway could be manipulated to treat gut microbiota-associated neurological disorders.

ACKNOWLEDGEMENTS

The authors are grateful to Drs. Hillary McGraw and Mark Cronan for sharing reagents; Drs. Herwig Baier, Claire Wyar, Albert Pan, Matthew Lovett-Barron, Drew Robson and Jennifer Li for sharing transgenic zebrafish lines; Dr. Vikas Gupta for generating *Tg(β-act2:Brainbow)* zebrafish and Dr. Valerie Tornini for generating *tph1b-/-* mutant zebrafish; Dr. Scott T. Espenschied, Dr. Jess McCann for providing technical assistance for FACS and bacterial culture; and ASR Business Partnering for scientific editing. The authors are also thankful for the Duke University Light Microscope Core Facility, Zebrafish Core Facility, and Sequencing and Genomic Technologies Shared Resource. This work was supported by National Institutes of Health grants R01-DK093399, R01-DK109368, Department of Veterans Affairs grant BX002230, and a Pew Scholars Innovation Award from the Pew Charitable Trusts. Sairam Jabba and Sven-Eric Jordt were supported by cooperative agreement U01ES030672 of the NIH CounterACT Program. Kenneth D. Poss was supported by R01 GM074057 and R35 HL150713. Lihua Ye was supported by the Digestive Disease and Nutrition Training Program at Duke University (NIH T32-DK007568). The lightsheet imaging was supported by the NIH Shared Instrumentation grant 1S10OD020010-01A1. The content is solely the responsibility of the authors and does not necessarily represent the views of the NIH.

AUTHOR CONTRIBUTIONS

Lihua Ye generated the hypotheses, conducted most of the experiments and wrote the manuscript. Munhyung Bae, Chelsi D. Cassilly and Jon Clardy conducted the *E. tarda* HPLC-MS analyses. Sairam V. Jabba and Sven-Eric Jordt conducted the mammalian Trpa1 fluorometric cell culture studies. Hsiu-Yi Lu conducted the *E. tarda* infection studies. Jinghu Wang, John Thompson and Ken Poss generated the *Tg(tph1b:mCherry-NTR)* and *TgBAC(gata5:RSD)* zebrafish lines. Colin Lickwar facilitated the RNA-seq analysis. Rodger Liddle and John Rawls directed the project and edited the manuscript.

DECLARATION OF INTERESTS

The authors declare no competing interests.

FIGURE LEGENDS

Figure 1. ***E. tarda* activates zebrafish EECs *in vivo*.** (A) Experimental approach for measuring EEC activity in free-swimming zebrafish. (B) Method for recording EEC responses to chemical and microbial stimulants in an EEC-CaMPARI model. (C-D) Confocal projection of mid-intestinal EECs upon water (C, negative control) or linoleate (D) stimulation in *Tg(neurod1:CaMPARI)* following UV-photoconversion. (E) Frequency distribution of EECs' red:green CaMPARI fluorescence intensity ratio in water or linoleate stimulated zebrafish. n=177 for water group and n=213 for linoleate group. (F) Percent EEC response in *Tg(neurod1:CaMPARI)* zebrafish. (G-H) Confocal projection of mid-intestinal EECs upon *Aeromonas* sp. ZOR0002 (G) or *E. tarda* FL6-60 (H) stimulation in *Tg(neurod1:CaMPARI)* following UV-photoconversion. (I) Frequency distribution of EECs' red:green CaMPARI fluorescence intensity ratio in zebrafish treated with water or *E. tarda*. n=117 for water group andn=156 for *E. tarda* group. (J) Representative heatmap image showing *Aeromonas* sp. ZOR0002, *Bacillus subtilis* 168 and *E. tarda* FL6-60 stimulated EEC red:green CaMPARI fluorescence ratio. (K) EEC activation in *Tg(neurod1:CaMPARI)* zebrafish stimulated with different bacterial strains. (L) Representative *Tg(neurod1:Gcamp6f)* zebrafish intestine stimulated with *E. tarda*. One-way ANOVA with Tukey's post-test was used in F and K for statistical analysis. *p<0.05; **p<0.01; ***p<0.001; ****p<0.0001.

Figure 2. ***E. tarda* activates EECs through Trpa1.** (A) Schematic diagram of zebrafish EEC RNA-seq. (B) Clustering of genes that are significantly enriched in zebrafish EECs and other IECs (P_{adj}<0.05). (C) Comparison of zebrafish and mouse EEC enriched genes. Published mouse EEC RNA-seq data was obtained from GSE114913 [26]. (D) Fluorescence image of *TgBAC(trpa1b:EGFP)*. Zoom-in view shows the expression of *trpa1b*+ cells in intestine. (E) Confocal projection of a *TgBAC(trpa1b:EGFP);Tg(neurod1:TagRFP)* zebrafish intestine. Yellow arrows indicate zebrafish EECs that are *trpa1b:EGFP*+. (F) Quantification of EEC Gcamp responses to Trpa1 agonist AITC stimulation in *trpa1b*+/+, *trpa1b*+/- and *trpa1b*-/- zebrafish. (G) Experimental design. (H-I) Confocal projection of *Tg(neurod1:CaMPARI)* zebrafish intestine stimulated with *E. tarda* with or without the Trpa1 antagonist HC030031. (J) Quantification of activated EECs in control and HC030031 treated zebrafish treated with water or *E. tarda*. (K) Experimental approach. (L-M) Confocal projection of *trpa1b*+/+ or *trpa1b*-/- *Tg(neurod1:CaMPARI)* intestine after stimulation with water or *E. tarda*. (N) Quantification of activated EEC percentage in WT and *trpa1b*-/- zebrafish treated with water or *E. tarda*. (O) Experimental design. (P-Q) Timed images of *trpa1b*+/+ or *trpa1b*-/- *Tg(neurod1:Gcamp6f)* zebrafish stimulated with *E. tarda*. (R) Quantification of relative EEC Gcamp6f fluorescence intensity in WT or *trpa1b*-/- zebrafish treated with *E. tarda*. One-way ANOVA with Tukey's post-test was used in F, J, N for statistical analysis. *p<0.05; **p<0.01; ***p<0.001; ****p<0.0001.

Figure 3. **Activation of EEC Trpa1 signaling facilitates enteric *E. tarda* clearance during infection.** (A) Schematic of *E. tarda* infection in zebrafish model. (B-C) Representative image of *trpa1b*+/+ or *trpa1b*-/- zebrafish infected with *E. tarda* expressing mCherry (*E. tarda* mCherry). (D) Quantification of *E. tarda* mCherry fluorescence in *trpa1b*+/+ or *trpa1b*-/- zebrafish intestine. (E) Quantification of intestinal *E. tarda* CFU in *trpa1b*+/+ or *trpa1b*-/- zebrafish. (F) Schematic of genetic model in which EECs are ablated via Cre-induced Diptheria Toxin (DTA) expression. (G) Representative image of *Tg(neurod1:cre; cmlc2:EGFP)* and *Tg(neurod1:cre; cmlc2:EGFP);*

TgBAC(gata5:RSD) with EECs that are labelled by *Tg(neurod1:EGFP)*. (H) Quantification of intestinal *E. tarda* CFU in WT or EEC ablated zebrafish. Student's t-test was used in D, E, H for statistical analysis. *p<0.05; ****p<0.0001.

Figure 4. **Activation of EEC Trpa1 signaling promotes intestinal motility.** (A) Illustration of EEC Trpa1 activation using an Optovin-UV platform. (B) Confocal image of *trpa1b*+/+ and *trpa1b*-/- *Tg(neurod1:Gcamp6f)* zebrafish EECs before and after UV activation. (C) Quantification of EEC Gcamp6f fluorescence changes in *trpa1b*+/+ and *trpa1b*-/- zebrafish before and after UV induction. (D) Representative images of *Tg(neurod1:Gcamp6f)* zebrafish intestine before and after UV-induced Trpa1 activation. Yellow arrowheads indicate the anterior to posterior movement of intestinal luminal contents from anterior to posterior following EEC activation. (E) PIV-Lab velocity analysis to quantify intestinal motility in WT and EEC ablated zebrafish. Spatiotemporal heatmap series represent the μ velocity of the imaged intestinal segment at the indicated timepoint post Trpa1 activation. (F) Quantification of the mean intestinal velocity magnitude before and after UV activation in WT and EEC ablated zebrafish. (G) Model of light activation of ChR2 in EECs. (H) Fluorescence image of *Tg(neurod1:Gal4); Tg(UAS:ChR2-mCherry)* zebrafish that express ChR2 in EECs. (I) Confocal image of ChR2 expressing EECs in *Tg(neurod1:Gcamp6f)* intestine before and after blue light-induced ChR2 activation. (J) Quantification of EEC Gcamp fluorescence intensity before and after blue light-induced ChR2 activation. (K) Magnitude of intestinal velocity before and after blue-light induced activation in ChR2+Trpa1+ EECs. (L) Mean velocity before and after blue light-induced activation in ChR2+Trpa1+ EECs. (M) Quantification of intestinal motility following *E. tarda* gavage. (N) Heatmap representing the velocity of the imaged intestinal segment at indicated timepoints following PBS or *E. tarda* gavage. (O) Mean intestinal velocity in zebrafish gavaged with PBS or *E. tarda*. Student's t-test was used in O for statistical analysis. ***p<0.001.

Figure 5. **Activation of EEC Trpa1 signaling activates enteric cholinergic neurons and promotes intestinal motility through 5-HT.** (A) Model: Trpa1 stimulation in EECs activates enteric neurons. (B) Confocal image of *ret*+/? (*ret*+/+ or *ret*+/-) and *ret*-/- intestine in *TgBAC(neurod1:EGFP);Tg(NBT:DsRed)* zebrafish. *neurod1* labelled EECs shown in green and *NBT* labelled ENS is shown in magenta. (C) Quantification of mean intestinal velocity before and after EEC Trpa1 activation in *ret*+/? zebrafish. (D) Quantification of mean intestinal velocity before and after UV activation in *ret*-/- zebrafish. (E) Confocal image of intestine in *TgBAC(chata:Gal4); Tg(UAS:NTR-mCherry)* zebrafish stained with 2F11. Cholinergic enteric neurons are shown in magenta and 2F11+ EECs are shown in green. (F) EECs (green) directly contact cholinergic enteric nerve fibers (magenta). Yellow arrows indicate the points where EECs form direct connections with *chata*+ ENS. (G) Confocal image of intestine in *TgBAC(chata:Gal4); Tg(UAS:NTR-mCherry); TgBAC(trpa1b:EGFP)* zebrafish. (H) Trpa1+EECs (green) form direct contact with *chata*+ enteric neurons (magenta). (I) Live imaging of *TgBAC(chata:Gal4); Tg(UAS:Gcamp6s); Tg(NBT:DsRed)* zebrafish intestine. All the enteric neurons are labelled as magenta by *NBT:DsRed*. Yellow arrow indicates a *chata*+ enteric neuron. (J) Lower magnifcation view of a *Gcamp6s* expressing *chata*+ enteric neuron. (K) *In vivo* calcium imaging of *chata*+ enteric neuron before and after EEC Trpa1 activation. (L) Quantification of *chata*+ enteric motor neuron Gcamp6s fluorescence intensity before and after EEC Trpa1 activation. (M) Confocal image of *TgBAC(trpa1b:EGFP)* zebrafish intestine stained for 5-HT. Yellow arrows indicate the presence of 5-HT in the basal area of *trpa1b*+ EECs. (N) Confocal image of *TgBAC(trpa1b:EGFP);Tg(tph1b:mCherry-NTR)* zebrafish intestine. Yellow arrow indicates the *trpa1b*+ EECs that express Tph1b. (O) Quantification of intestinal motility changes in response to

EEC Trpa1 activation in *tph1b*+/- and *tph1b*-/- zebrafish. Student's t test was used in O for statistical analysis. **p<0.01

Figure 6. **EEC Trpa1 signaling activates vagal sensory ganglia.** (A) Hypothetical model. (B) Confocal image of zebrafish vagal sensory ganglia labelled with *Tg(neurod1:EGFP)* (green) and acetylated αTubulin antibody staining (magenta). (C) Lightsheet projection of zebrafish stained acetylated αTubulin antibody. Yellow arrow indicates vagal nerve innervation to the intestine. (D) *neurod1:EGFP*+ EECs (green) directly contact vagal sensory nerve fibers labelled with αTubulin (white). (E) Confocal image of the vagal sensory nucleus in zebrafish larvae hindbrain where - vagal sensory neuron project. Vagal sensory nerve fibers are labeled with different fluorophores through Cre-brainbow recombination in *Tg(neurod1:cre); Tg(βact2:Brainbow)* zebrafish. The 3D zebrafish brain image is generated using mapzebrain [85]. (F) Confocal image of vagal sensory ganglia in *Tg(neurod1:cre); Tg(βact2:Brainbow)* zebrafish. Asterisk indicates posterior lateral line afferent nerve fibers. Blue arrowheads indicate three branches from vagal sensory ganglia that project to the hindbrain. (G) Confocal image demonstrates the EEC-vagal network in *Tg(isl1:EGFP); Tg(neurod1:TagRFP)* zebrafish intestine. EECs are labeled as magenta by *neurod1:TagRFP* and the vagus nerve is labeled green by *isl1:EGFP*. (H) EECs (*neurod*1+; magenta) directly contact vagal nerve fibers (*isl1*+; green). Yellow arrows indicate the points where EECs form direct connections with vagal nerve fibers. (I-J) *In vivo* calcium imaging of vagal sensory ganglia in *Tg(neurod1:Gcamp6f); Tg(NBT:DsRed)* zebrafish gavaged with PBS (I) or *E. tarda* (J). (K) Quantification of individual vagal sensory neuron Gcamp6f fluorescence intensity in *E. tarda* or PBS gavaged zebrafish. (L-N) Confocal image of vagal ganglia stained with p-ERK antibody in WT or EEC ablated zebrafish gavaged with PBS or Trpa1 agonist AITC. The vagal sensory ganglia expressing *neurod1:EGFP* are labeled green and activated vagal sensory neurons are labeled magenta by p-ERK antibody staining. (O-Q) Confocal projection of vagal ganglia stained with p-ERK antibody in WT or EEC ablated zebrafish gavaged with PBS or *E. tarda*. (R) Quantification of p-ERK+ vagal sensory neurons in WT or EEC ablated zebrafish following PBS or AITC gavage. (S) Quantification of p-ERK+ vagal sensory neurons in WT or EEC ablated zebrafish following PBS or *E. tarda* gavage. (T) Quantification of p-ERK+ vagal sensory neurons in WT or *trpa1b*-/- zebrafish following *E. tarda* gavage. One-way ANOVA with Tukey's post test was used in R and S and Student's t-test was used in T for statistical analysis. *p<0.05; **p<0.01; ***p<0.001; ****p<0.0001.

Figure 7. *E. tarda* derived Tryptophan catabolites activate Trpa1 and the EEC-vagal pathway. (A) Method for preparing different fractions from *E. tarda* GZM (zebrafish water) culture. (B) Activated EECs in *Tg(neurod1:CaMPARI)* zebrafish stimulated by different *E. tarda* fractions. (C) Activated EECs in *trpa1b*+/+ and *trpa1b*-/- *Tg(neurod1:CaMPARI)* zebrafish stimulated with *E. tarda* CFS. (D) Screening of supernatants of *E. tarda* in GZM culture broths by HPLC-MS. Samples were collected at 0, 1, 6, 24 h. Abbreviations are as follows: IAld, indole-3-carboxaldehyde; and IEt, tryptophol. Extracted ions were selected for IAld (m/z 145), IEt, (m/z 161), and Indole (m/z 117). (E-F) *Tg(neurod1:Gcamp6f)* zebrafish stimulated by Indole or IAld. Activated EECs in the intestine are labelled with white arrows. (G) EEC Gcamp fluorescence intensity in *Tg(neurod1:Gcamp6f)* zebrafish stimulated with different tryptophan catabolites. (H) Quantification of EEC Gcamp activity in *trpa1b*+/+ and *trpa1b*-/- *Tg(neurod1:Gcamp6f)* zebrafish stimulated with Indole or IAld. (I-J) Indole (I) and IAld (J) stimulation of Ca^{2+} influx in human TRPA1 expressing HEK-293T cells, measured as fluorescence increase of intracellular Calcium 6 indicator. (K) Dose-response analysis of A967079 inhibition of Indole and IAld induced Ca^{2+} influx. (IC_{50} = 149.6 nM, 131.3-170.8 nM 95% CI for Indole; and, IC_{50} = 158.1 nM, 135.4 – 185.6 μM 95%

CI for IAld). Concentration-response data of A967079 inhibition was normalized to response elicited by 100 µM agonist (Indole or IAld). (L-O) *In vivo* calcium imaging of vagal sensory ganglia in WT or EEC ablated *Tg(neurod1:Gcamp6f); Tg(neurod1:TagRFP)* zebrafish gavaged with PBS, Indole or IAld. (P) Quantification of whole vagal sensory ganglia Gcamp6f fluorescence intensity in WT or EEC ablated zebrafish gavaged with PBS or Indole. (R) Proposed model for *E. tarda* derived tryptophan catabolites activating a gut-brain pathway through EEC-ENS and EEC-vagal communication. One-way ANOVA with Tukey's post test was used in B and Q and Student's t-test was used in C, H for statistical analysis. *p<0.05; **p<0.01; ***p<0.001; ****p<0.0001.

SUPPLEMENTAL FIGURES

Figure S1. *E. tarda* activates EECs *in vivo*. (A) Epifluorescence image of *Tg(neurod1:CaMPARI)* zebrafish without UV conversion. Note that there is no red CaMPARI signal (magenta) in A'. (B) Confocal image of intestinal EECs in *Tg(neurod1:CaMPARI)* zebrafish without UV conversion. (C) Epifluorescence image of unstimulated *Tg(neurod1:CaMPARI)* zebrafish post UV conversion. The red CaMPARI signal is apparent in CNS and islets in C'. (D-F') Confocal image of intestinal EECs (D, D'), CNS (E, E') and islets (F, F') in unstimulated *Tg(neurod1:CaMPARI)* zebrafish after UV conversion. (G-I) Quantification of EEC red:green CaMPARI fluorescence ratio in water- and linoleate-stimulated zebrafish. (L) Schematic of *in vivo* EEC Gcamp recording in response to bacterial stimulation in *Tg(neurod1:Gcamp6f)* zebrafish. (M) Quantification of EEC Gcamp6f fluorescence in response to stimulation by different bacteria. (N) Quantification of EEC Gcamp6f fluorescence before and 20 mins after *E. tarda* administration. (O-P) Fluorescence image of zebrafish intestine in *Tg(neurod1:Gcamp6f)* zebrafish without treatment (O) or 5 hours post *E. tarda* infection (P). (Q) Quantification of EEC Gcamp6f fluorescence in zebrafish without or with *E. tarda* infection. Student's t-test was used in N and Q for statistical analysis. * p<0.05.

Figure S2. **Conserved genetic features between zebrafish and mammalian EECs.** (A) FACS was used to isolate EECs (*cldn15la:EGFP*+; *neurod1:TagRFP*+) and other IECs (*cldn15la:EGFP*+; *neurod1:TagRFP*-) in *TgBAC(cldn15la:EGFP)*; *Tg(neurod1:TagRFP)* zebrafish. (B) Gel image of the PCR product from FACS sorted cell population using primers for *18S* (house keeping gene), *pyyb* (EEC marker), *fabp2* (enterocyte marker) and *agr2* (EEC progenitor and goblet cell marker). (C) Gene Ontology analysis of genes that were significantly enriched in zebrafish EEC population (P_{FDR}<0.05). (D) Log2 fold change of genes that encode hormones, transcription factors, cell surface receptors, and membrane ion channels in zebrafish, mouse, and human EECs. Both mouse and human EEC data were reanalyzed from a previous publication (human, GSE114853; mouse, GSE114913) [26]. The red color labelled genes are shared EEC genes among zebrafish, mouse and human. (E) The gene list of EEC subpopulation markers that were enriched in zebrafish EECs (log_2EEC/IEC>1). The asterisk indicates marker genes that were significantly enriched in zebrafish EECs (p<0.05). The EEC subpopulation marker genes were identified in a published mouse small intestinal epithelium single cell sequencing study [27]. Progenitor-A (EEC progenitor that express Ghrl), SAKD ($Sct^+Ghrl^+GIP^+Sst^+$ EECs), SILA ($Sct^+Cck^+Gcg^+Ghrl^+$ EECs), SIK ($Sct^+Cck^+GIP^+$ EECs), SIK-P ($Sct^+Cck^+GIP^+$ EEC progenitors), SIL-P ($Sct^+Cck^+Gcg^+$ EEC progenitors), SIN ($Sct^+Cck^+Nts^+$ EECs), EC (enterochromaffin cells). secretin (Sct)-S, cholecystokinin (Cck)-I, proglucagon (Gcg)-L, glucose-dependent insulinotropic polypeptide (GIP)-K, somatostatin (Sst)-D, neurotensin (Nts)-N, ghrelin (Ghrl)-A.

Figure S3. EECs express *trpa1b* and respond to Trpa1 agonist. (A) Plot of log_2FoldChange against log_{10}NormalizedCounts showing the expression of *trpa1a* and *trpa1b* genes in zebrafish EEC RNA-seq data. (B) Normalized counts of *trpa1a* and *trpa1b* gene expression in zebrafish

EECs and other IECs. (C) Gel image of PCR product from FACS sorted EECs and other IECs cell population using primers from *trpa1a*, *trpa1b* and *18S*. (D-E) Epifluorescence image of *trpa1b*+/+ (D) and *trpa1b*-/- (E) *Tg(neurod1:Gcamp6f)* zebrafish before or 2 mins post Trpa1 agonist AITC stimulation. (F) Confocal projection of *trpa1b*+/+ and *trpa1b*-/- *Tg(neurod1:CaMPARI)* zebrafish after AITC stimulation and UV light photoconversion. (G) Epifluorescence image of *Tg(neurod1:Gcamp6f)* zebrafish following AITC stimulation with or without Trpa1 antagonist HC030031 treatment. (H) Epifluorescence image of *trpa1a*+/+ and *trpa1a*-/- *Tg(neurod1:Gcamp6f)* zebrafish 2 mins after AITC stimulation. (I) Quantification of EEC Gcamp fluorescence signal in *trpa1a*+/+, *trpa1a*+/- and trpa1a-/- zebrafish. (J) Plot of $\log_2$FoldChange against $\log_{10}$NormalizedCounts showing the expression of cytokine and cytokine receptor genes (blue dots) and microbial pattern recognition receptor genes (MPRR, red dots) in zebrafish EEC RNA-seq analysis. (K-L) Normalized counts of MPRR genes and cytokine receptor genes in EECs and other IECs sample groups. One-way ANOVA with Tukey's post test was used in I for statistical analysis.

Figure S4. The effects of *trpa1b* and EEC ablation on gut bacterial burden in the conventionalized or *E. tarda*-treated state. (A) Model of gut bacterial CFU quantification. (B) Quantification of gut bacterial CFU in *trpa1b*+/+, *trpa1b*+/- and *trpa1b*-/- conventionalized zebrafish. (C) Epifluorescence image of WT, *Tg(neurod1:cre)*, *Tg(gata5:RSD)* and *Tg(neurod1:cre); Tg(gata5:RSD)* zebrafish. The EECs in all the groups are labelled by *Tg(neurod1:EGFP)*. Note that *neurod1:EGFP* labelling is largely absent in *Tg(neurod1:cre); Tg(gata5:RSD)* zebrafish indicating EEC ablation. (D-E) Confocal images of *Tg(neurod1:cre)* (D) and *Tg(neurod1:cre); Tg(gata5:RSD)* (E) zebrafish intestine stained with PYY antibody. Yellow arrows in D indicate PYY+ EECs. (F) qPCR analysis of EEC marker genes, other IEC marker genes and neuronal genes in WT and EEC-ablated zebrafish. (G) Quantification of gut bacterial CFU in WT, *Tg(neurod1:cre)*, *Tg(gata5:RSD)* and *Tg(neurod1:cre); Tg(gata5:RSD)* conventionalized zebrafish. (H) Epifluorescence image of *Tg(gata5:RSD)* and EEC-ablated zebrafish infected with *E. tarda* mCherry. (I) Quantification of *E. tarda* mCherry fluorescence intensity in the intestinal lumen of *Tg(gata5:RSD)* or EEC-ablated zebrafish. One-way ANOVA with Tukey's post test was used in B, F and G and student t-test was used in I for statistic analysis. *$p<0.05$, **$p<0.01$, ***$p<0.001$.

Figure S5. Activation of EEC Trpa1 signaling promotes intestinal motility. (A) Experimental design for activating EEC Trpa1 signaling using Optovin-UV. (B-C) Confocal image of *Tg(neurod1:Gcamp6f); Tg(neurod1:TagRFP)* zebrafish intestine before (B) and after (C) UV light activation. Yellow arrows indicate the subpopulation of EECs exhibiting increased Gcamp fluorescence following UV activation. (D) Quantification of the EEC Gcamp6f to TagRFP fluorescence ratio before and after UV activation. (E-G) Quantification of intestinal motility using PIV-LAB velocity analysis before and after UV activation. Note that Optovin-UV induced Trpa1 activation increased μ velocity (horizontal movement) more than v velocity (vertical movement). (H-I) Confocal image of ChR2+Trpa1+ EECs (yellow circles, H) and ChR2+Trpa1- EECs (red circles, I) in *TgBAC(trpa1b:EGFP); Tg(neurod1:Gal4); Tg(UAS:ChR2-mCherry)* zebrafish. (J) Quantification of μ velocity following blue light activation of ChR2+Trpa1+ or ChR2+Trpa1- EECs. (K) Quantification of mean intestinal velocity change before and after blue light activation of ChR2+Trpa1- EECs.

Figure S6. The enteric nervous system in EEC Trpa1-induced intestinal motility. (A-B) Epifluorescence image of *ret+/+ or ret+/-* (*ret+/?*, A) and *ret-/-* (B) *Tg(NBT:DsRed);*

Tg(neurod1:EGFP) zebrafish. The intestines are denoted by white dash lines. (C-D) Epifluorescence image of *ret*+/? *Tg(neurod1:Gcamp6f)* zebrafish before (C) and 2 mins after AITC stimulation (D). (E-F) Epifluorescence image of *ret*-/- *Tg(neurod1:Gcamp6f)* zebrafish before (E) and 2 mins after AITC stimulation (F). (G) Quantification of *ret*+/? and *ret*-/- intestinal µ velocity following Optovin-UV-induced Trpa1 activation. (H) Quantification of velocity before and after Optovin-UV-induced Trpa1 activation in *ret*+/? and *ret*-/- zebrafish. (I-J) Confocal projection of *sox10*+/? zebrafish intestine stained with Zn12 (I, magenta, ENS labeling) or 2F11(J, green, EEC labeling). (K-L) Confocal projection of *sox10*-/- zebrafish intestine stained with zn-12 (K) or 2F11(L). (M-N) Quantification of changes in mean intestinal velocity before and after Optovin-UV activation in *sox10*+/? (M) or *sox10*-/- (N) zebrafish. (O-P) Confocal projection of *TgBAC(trpa1b:EGFP)* zebrafish intestine stained with Desmin (myoblast or smooth muscle cell marker, O') or Zn12 (ENS marker, P'). (Q) Confocal image of *TgBAC(trpa1b:EGFP); Tg(NBT:DsRed)* zebrafish intestine. Note in P and Q that both Zn12+ ENS and NBT+ ENS are *trpa1b*-. (R) Confocal image of *TgBAC(chata:Gal4); Tg(UAS:NTR-mCherry)* zebrafish intestine stained with Zn12 (green). Yellow arrows indicate the cell body of chata+ enteric neurons. (S) Confocal image of *TgBAC(chata:Gal4); Tg(UAS:NTR-mCherry); TgBAC(trpa1b:EGFP)* zebrafish intestine. Note that the *chata*+ ENS are *trpa1b*-.

Figure S7. Zebrafish EECs exhibit conserved presynaptic markers and 5-HT expression. (A-B) Confocal projection of 6 dpf (A) and adult (B) *Tg(neurod1:EGFP)* zebrafish intestine stained with the neuronal marker synaptic vesical protein 2 (SV2, magenta)) antibody. (C) Lower magnification view of an EEC that exhibiting a neuropod contacting SV2 labelled neurons in the intestine. Yellow arrow indicates the EEC neuropod is enriched in SV2. (D) Lower magnification view of an EEC and neuropod in *Tg(neurod1:TagRPF); Tg(neurod1:mitoEOS)* zebrafish. The yellow arrow indicates the EEC neuropod is enriched in mitochondria (green, labelled by *neurod1:mitoEOS*). (E) Confocal image of EECs (2F11+, green) and Chata+ enteric nerve fibers (magenta) in *TgBAC(chata:Gal4); Tg(UAS: NTR-mCherry)* zebrafish. Yellow arrows indicate the connection between EECs and Chata+ ENS fibers. (F-G) Confocal image showing the direct contact of EECs with Chata+ enteric nerve fibers. (H) Log2 fold change of presynaptic genes in zebrafish, mouse and human EECs. (I) Schematic model showing the proposed function of presynaptic genes in EECs. The core synaptic vesicle genes are labelled blue in H. (J-K) Confocal image and lower magnification view of *TgBAC(trpa1b:EGFP); Tg(tph1b:mCherry-NTR)* zebrafish intestine showing the *tph1b*+ (magenta) *trpa1b*+ (green). (L) Quantification of *tph1a* and *tph1b* in zebrafish EECs. (M) Quantification of 5-HT+ or *tph1b*+ EECs. (N) Quantification of *tph1b*+ and *trpa1b*+ EECs. Note the majority of *tph1b*+ EECs are *trpa1b*+. (O) Quantification of mean intestinal µ velocity in *tph1b*+/- and *tph1b*-/- zebrafish.

Figure S8. Zebrafish vagal sensory nerve innervate the intestine. (A-B) Lightsheet imaging of the right (A) and left (B) side of zebrafish intestine stained with acylated α-tubulin antibody (white). (C) Schematic diagram of the vagal-brainbow model to label vagal sensory cells using *Tg(neurod1:cre); Tg(βact2:Brainbow)* zebrafish. See vagal-Brainbow projection in Fig. 6F. (D) Confocal image of vagal ganglia in brainbow zebrafish stained with GFP antibody (green). Note that GFP antibody recognizes both YFP+ and CFP+ vagal sensory neurons. Six branches (V_i to V_{vi}) extend from the vagal sensory ganglia and branch V_{vi} innervates the intestine. (E-E') Confocal image of vagal sensory ganglia in brainbow zebrafish showing that V_{vi} exits from the ganglia and courses behind the esophagus. (F-G) Confocal image of the proximal (F) and distal (G) intestine in brainbow zebrafish. The vagus nerve (green) innervates both intestinal regions. (H) Confocal image of vagal sensory ganglia in *Tg(isl1:EGFP); Tg(neurod1:TagRFP)* zebrafish. (I) Confocal

image of intestine in *Tg(isl1:EGFP); Tg(neurod1:TagRFP)* zebrafish. The vagus nerve is labelled by *isl1* (green) and the intestinal EECs are labelled by *neurod1* (magenta). (J) Confocal plane of intestine in *Tg(isl1:EGFP); Tg(neurod1:TagRFP)* zebrafish. Note that the V_{vi} branch of the vagus nerve is labelled by isl1 and travels behind the esophagus to innervate the intestine. (K) Schematic of *in vivo* vagal calcium imaging in PBS or AITC gavaged zebrafish. (L) *In vivo* vagal calcium imaging of *Tg(neurod1:TagRFP); Tg(neurod1:Gcamp6f)* zebrafish without gavage, gavaged with PBS or gavaged with AITC.

Figure S9. *E. tarda* derived tryptophan catabolites activate Trpa1. (A) Chemical profiles of Trp-Indole derivatives from supernatants of *E. tarda* in TSB medium. (B) Screening of supernants of *E. tarda* in TSB culture broth. Samples for *E. tarda* in TSB culture were collected at 0, 6, 18, and 24 h. (C) Screening of supernatants of *E. tarda* in TSB culture broth. Abbreviations are as follows: IAld, indole-3-carboxaldehyde; IEt, tryptophol; IAM, indole-3-acetamide; IAA, indole-3-acetic acid; IAAld, indole-3-acetaldehyde; and IpyA, indole-3-pyruvate. Extracted ions were selected for IAld (m/z 145), IEt, (m/z 161), Indole (m/z 117), IAAld (m/z 159), IAM (m/z 174), IAA (m/z 175), and IpyA (m/z 203). (D) Proposed model of *E. tarda* tryptophan catabolism. (E) Indole concentrations from supernatants of different bacterial strains in 1h TSB or GZM culture broth. (F) Dose-response analysis of the integrated Calcium 6 fluorescence response above baseline (Fmax-F0; maximal change in Ca^{2+} influx) as a function of indole and IAld concentration in human TRPA1 expressing HEK-293T cells. (EC_{50} = 88.7 µM, 68.2-114.7 µM 95% CI for indole; and, EC_{50} = 77.7 µM, 66.8-91.8 µM 95% CI for IAld). Concentration-response data were normalized to 1 mM cinnamaldehyde (CAD), a known TRPA1 agonist. Data represent the mean of 3-4 experiments performed with 3-4 replicates. (G-H) Effects of TRPA1 inhibition using various concentrations of inhibitor A967079, on subsequent Ca^{2+} influx in response to indole (100 µM, G) or, IAld (100 µM, H) in human TRPA1 expressing HEK-293T cells. Data are from a representative experiment performed in triplicate and repeated three times. (I-J) Sensitivity of mouse TRPA1 to indole and IAld. (I) Dose-response effects of indole and IAld (EC50 = 130.7 µM, 107.8 – 158.4 µM 95% CI for Indole; and, EC50 = 189.0 µM, 132.8 - 268.8 µM 95% CI for IAld). Concentration-response data were normalized to 1 mM cinnamaldehyde (CAD), a known TRPA1 agonist. (J) Effects of the Trpa1 inhibitor A967079, on $[Ca^{2+}]_i$ in response to 100 µM indole in mouse Trpa1-expressing HEK-293T cells. Cells were treated with A967079 before the addition of indole (100 µM). Changes in Calcium 6 fluorescence above baseline (Fmax-F0; maximal $[Ca^{2+}]_i$) are expressed as a function of Trpa1 inhibitor, A967079, concentration (IC50 = 315.5 nM, 202.3 – 702.3 nM 95% CI for indole). Concentration-response data were normalized to the response elicited by 100 µM Indole. Data represent mean ± s.e of normalized measures pooled from two experiments, each performed in triplicate. (K) Experimental model for measuring intestinal motility in response to indole stimulation. (L) EEC Gcamp6f fluorescence (blue line) and changes in intestinal motility (heat map) following indole stimulation. (M) Intestinal µ velocity in response to PBS or indole stimulation. (N) Mean intestinal velocity magnitude 0-50s and 200-250s following indole stimulation.

Table S1. Key resources.

Table S2. Zebrafish EEC RNA-seq data analyzed by DEseq2.

Table S3. Comparison of zebrafish EECs with human and mouse EECs using RNA-seq.

Table S4. Expression of hormones, transcription factors, receptors, and innate immune genes in EECs and other IECs.

Video 1. *E. tarda* activates EECs *in vivo*. Time-course video of *Tg(neurod1:Gcamp6f)* zebrafish that are stimulated with *E. tarda* bacteria. Anterior is to the right, and dorsal is to the top.

Video 2. Trpa1 agonist activates EECs in vivo. Time-course videos of *trpa1b*+/+ and *trpa1b*-/- *Tg(neurod1:Gcamp6f)* zebrafish that are stimulated with Trpa1 agonist AITC. Anterior is to the right, and dorsal is to the top.

Video 3. Optovin-UV activates EECs. Time-course video of *Tg(neurod1:Gcamp6f); Tg(neurod1:TagRFP)* zebrafish before and post Optovin-UV induced EEC Trpa1 activation. Anterior is to the left, and dorsal is to the bottom.

Video 4. Activation of EEC Trpa1 in control zebrafish increases intestinal motility. Time-course video of *Tg(neurod1:Gcamp6f)* WT zebrafish before and post Optovin-UV induced EEC Trpa1 activation. Anterior is to the left, and dorsal is to the top.

Video 5. Activation of EEC Trpa1 in EEC ablated zebrafish does not increase intestinal motility. Time-course video of *Tg(neurod1:Gcamp6f)* EEC ablated zebrafish before and post Optovin-UV induced EEC Trpa1 activation. Anterior is to the left, and dorsal is to the top.

Video 6. Optic EEC activation in EEC-ChR2 expressing transgenic zebrafish. Time-course video of *Tg(neurod1:Gcamp6f); Tg(neurod1:Gal4); Tg(UAS:ChR2-mCherry)* zebrafish before and post yellow light induced EEC activation. Anterior is to the left, and dorsal is to the bottom.

Video 7. Activation of Trpa1+EECs increases intestine motility. Time-course videos of *TgBAC(trpa1b:EGFP); Tg(neurod1:Gal4); Tg(UAS:ChR2-mCherry)* before and post optic activation of Trpa1-EECs and Trpa1+ EECs. The yellow light was delivered specifically to the selected EECs to activate the ChR2 channel. Note that the first frame in each video shows the EGFP channel to identify EECs that do or do not express *trpa1b*. Anterior is to the left, and dorsal is to the bottom.

Video 8. *E. tarda* increases intestinal motility. Time-course videos of WT zebrafish 30 mins post PBS or *E. tarda* gavage. Anterior is to the left, and dorsal is to the top.

Video 9. EECs physically connect to Chata+ enteric neurons. 3D-reconstruction of *Tg(chata: NTR-mCherry)* zebrafish intestine stained with 2F11 antibody that labels EEC. The Chata+ nerve is shown as magenta and the EECs are shown as green.

Video 10. Activation of EEC Trpa1 increases Chata+ ENS calcium. Time-course videos of *TgBAC(chata:Gal4); Tg(UAS;Gcamp6s)* that before and post Optovin-UV induced EEC Trpa1 activation. Anterior is to the left, and dorsal is to the top.

Video 11. *E. tarda* increases vagal ganglia calcium. Time-course videos of vagal ganglia calcium in *Tg(neurod1:Gcamp6f); Tg(neurod1:TagRFP)* zebrafish that are gavaged PBS or *E. tarda*. Anterior is to the left, and dorsal is to the top.

Video 12. IAld activates EECs *in vivo*. Time-course videos of *trpa1b*+/+ (WT) and *trpa1b*-/- *Tg(neurod1:Gcamp6f)* zebrafish that are stimulated with IAld. Note that there is a basal amount of intestinal motility associated with this methylcellulose preparation that is retained in vehicle-only negative controls (not shown) and in trpa1b mutants. Anterior is to the right, and dorsal is to the top.

Video 13. Indole activates EECs *in vivo*. Time-course videos of *trpa1b*+/+ (WT) and *trpa1b*-/- *Tg(neurod1:Gcamp6f)* zebrafish that are stimulated with indole. Note that there is a basal amount of intestinal motility associated with this methylcellulose preparation that is retained in vehicle-only negative controls (not shown) and in trpa1b mutants. Anterior is to the right, and dorsal is to the top.

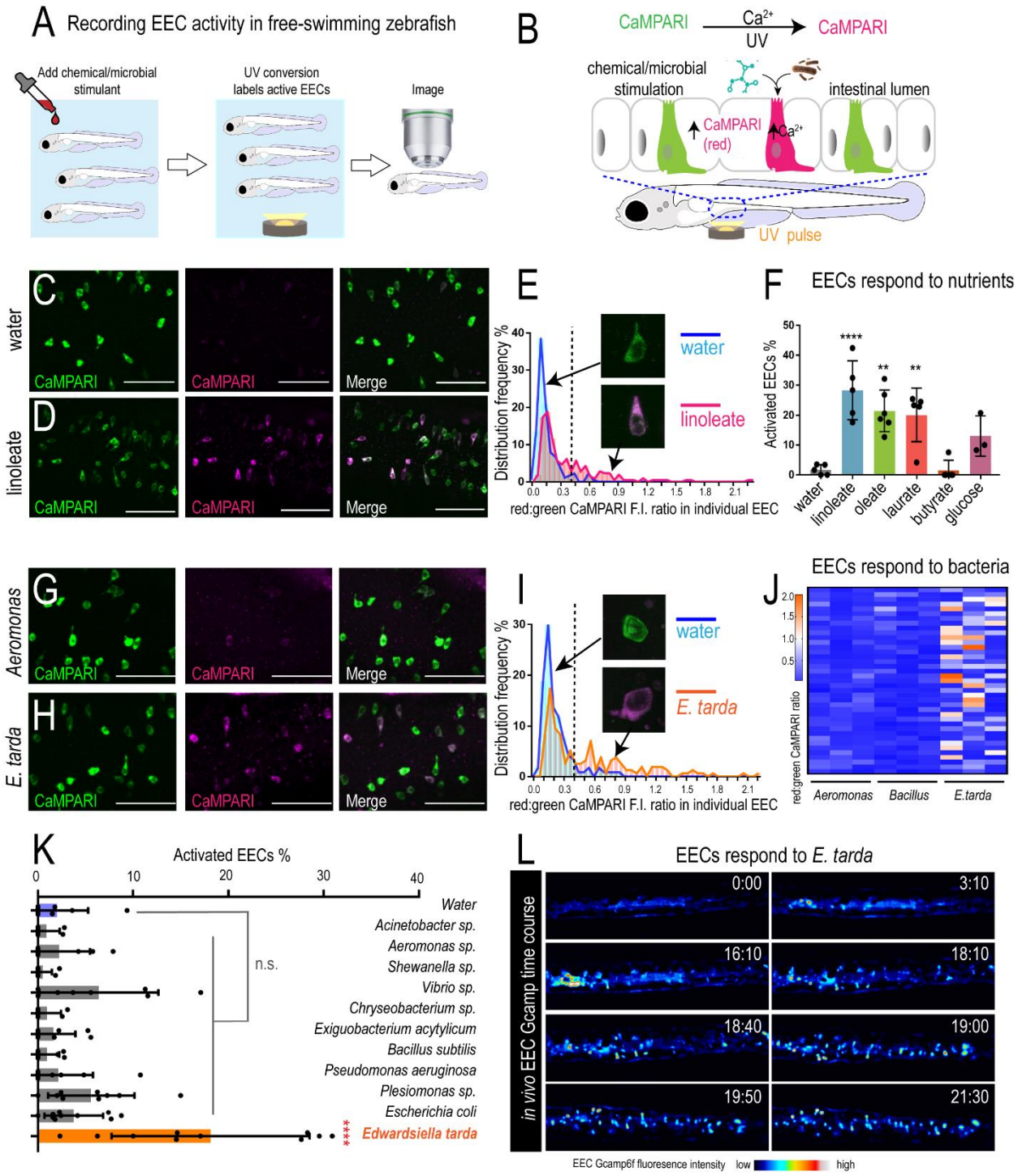

Figure 1. ***E. tarda* activates zebrafish EECs *in vivo*.**

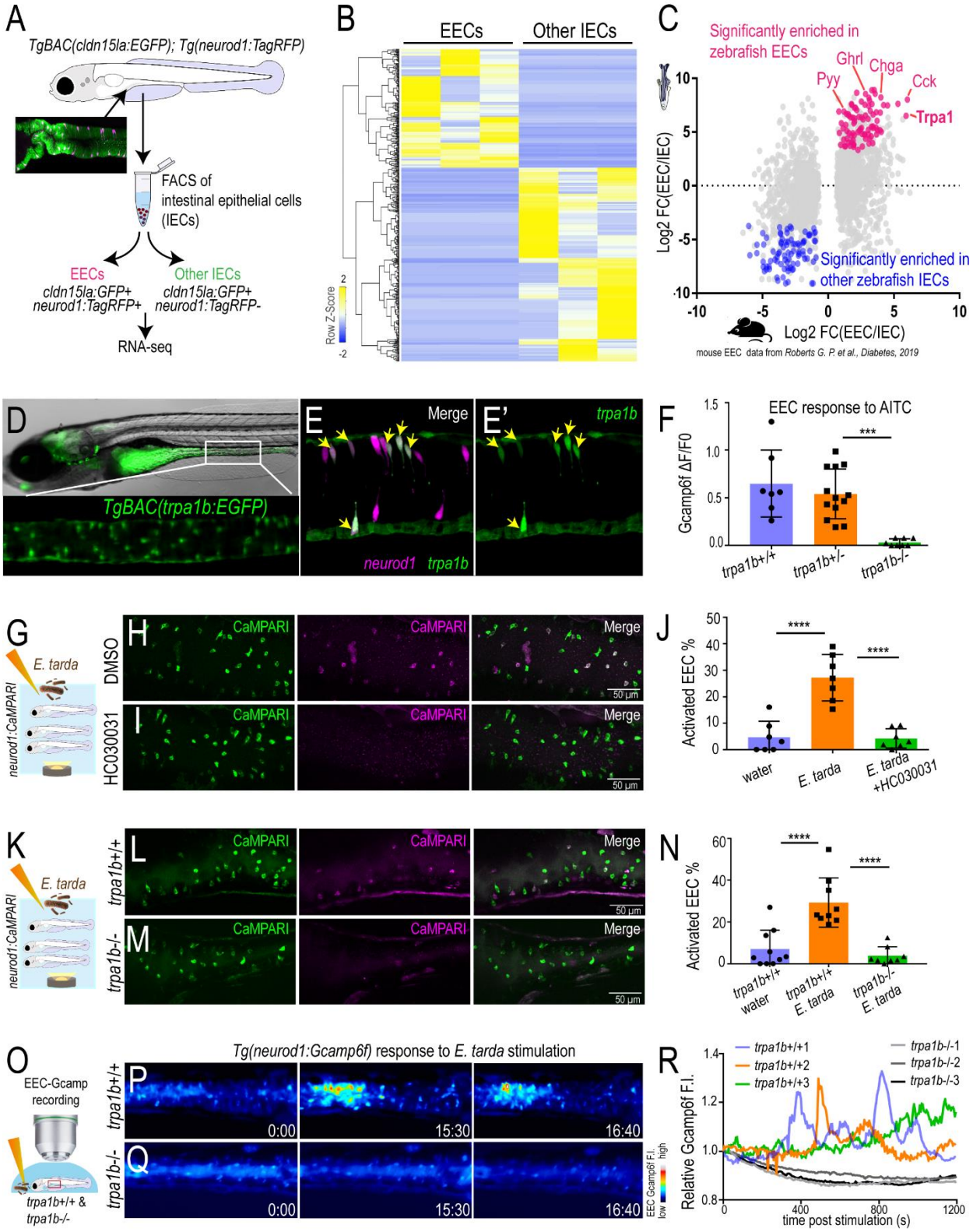

Figure 2. ***E. tarda*** **activates EECs through Trpa1.**

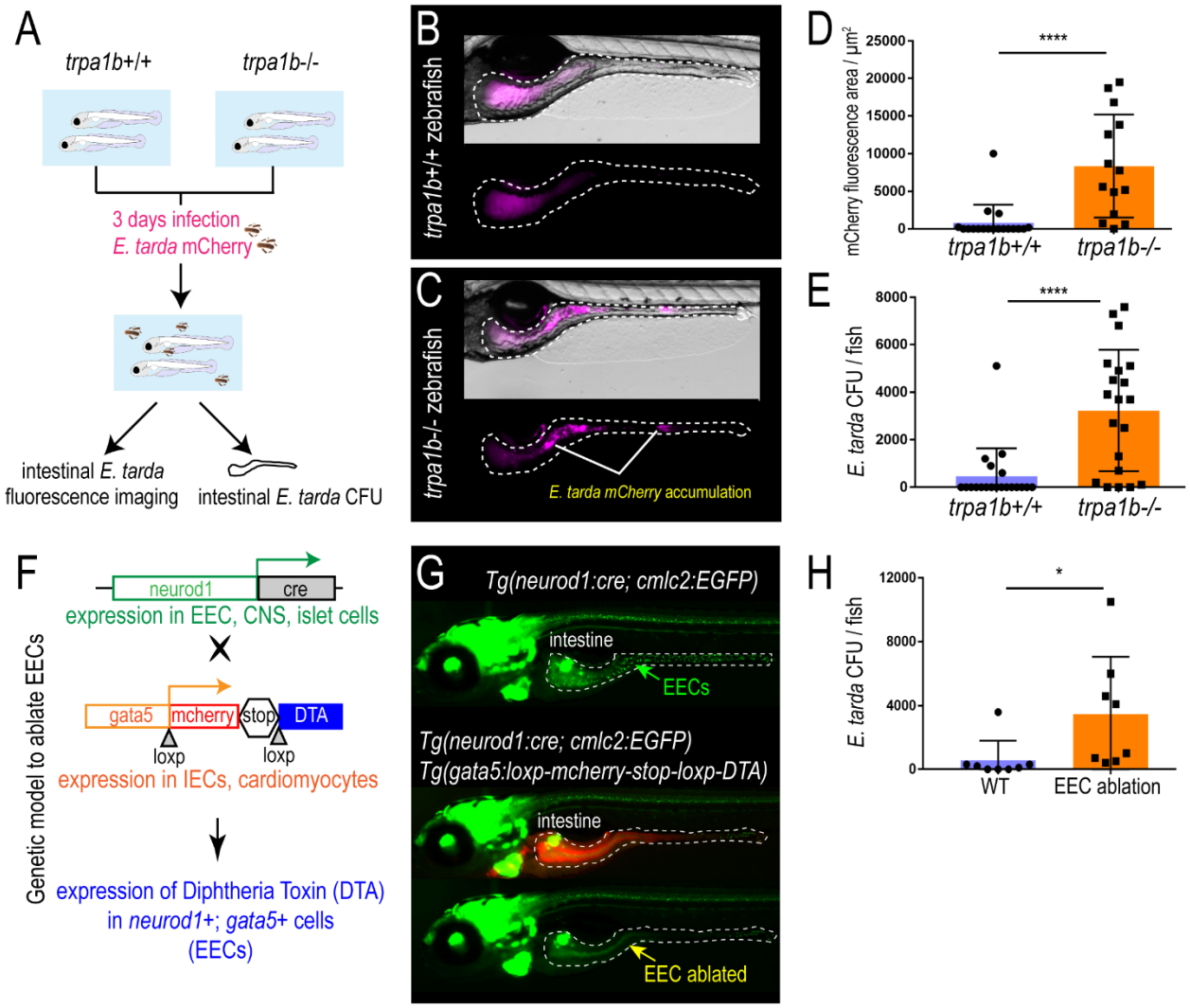

Figure 3. Activation of EEC Trpa1 signaling facilitates enteric *E. tarda* clearance during infection.

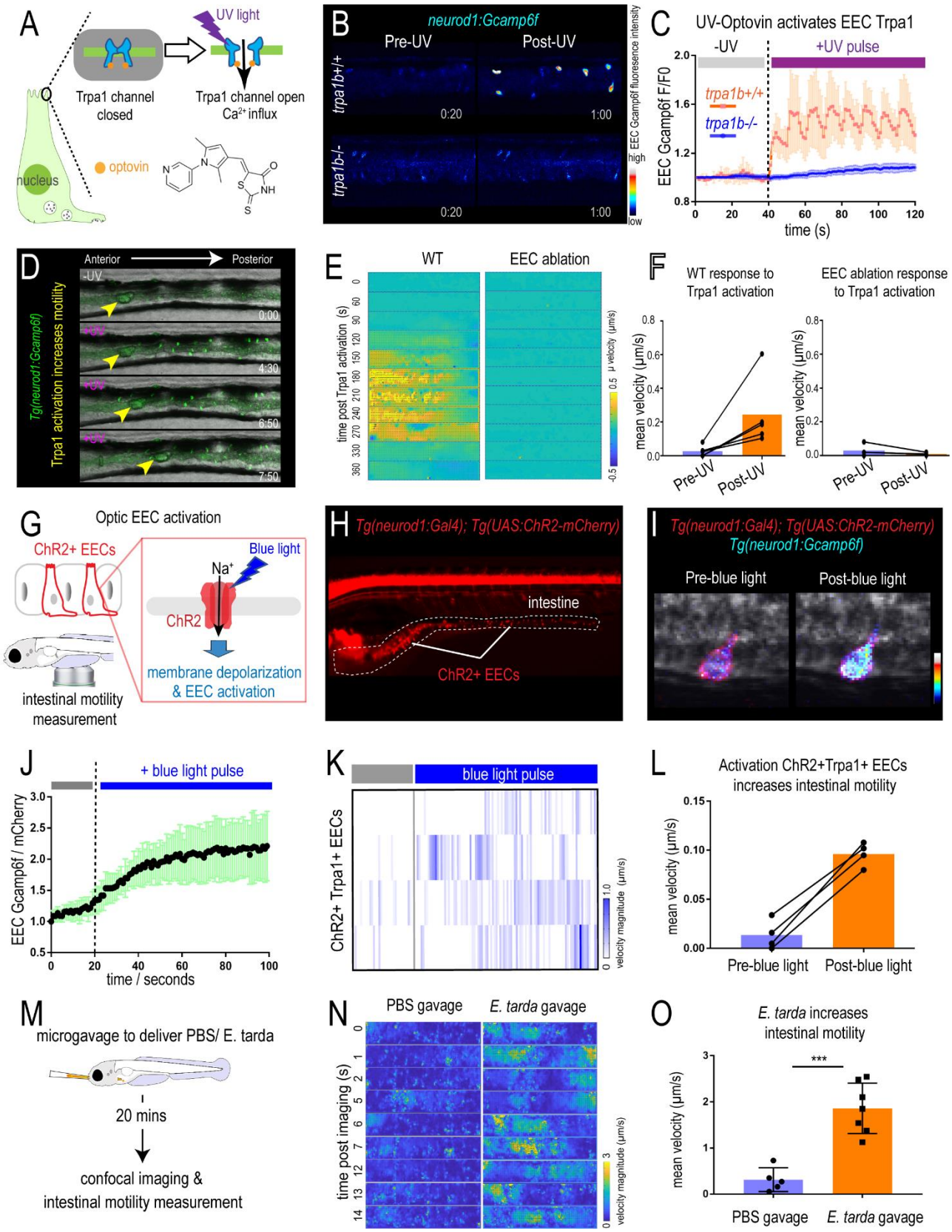

Figure 4. Activation of EEC Trpa1 signaling promotes intestinal motility.

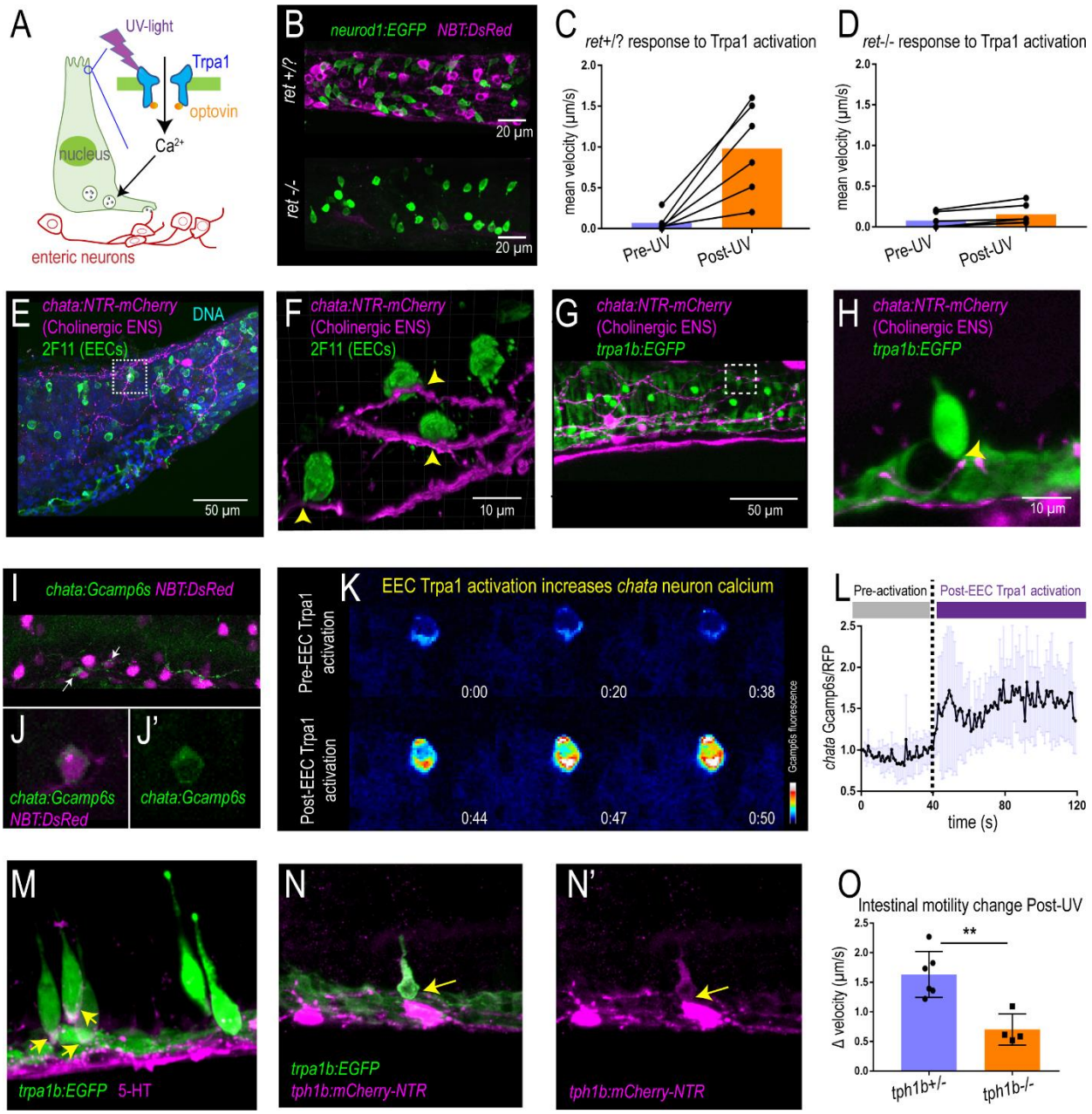

Figure 5. Activation of EEC Trpa1 signaling activates enteric cholinergic neurons and promotes intestinal motility through 5-HT.

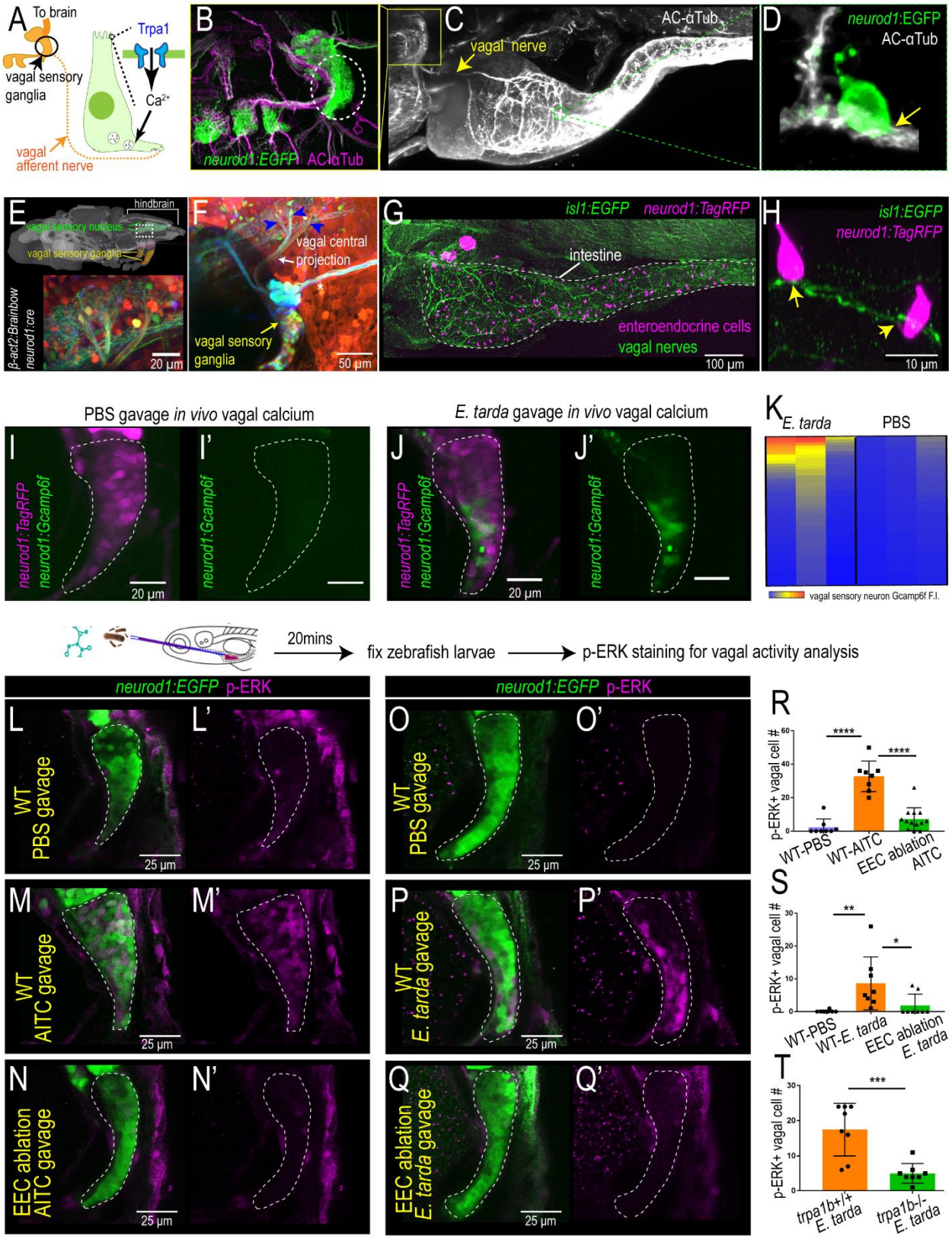

Figure 6. **EEC Trpa1 signaling activates vagal sensory ganglia.**

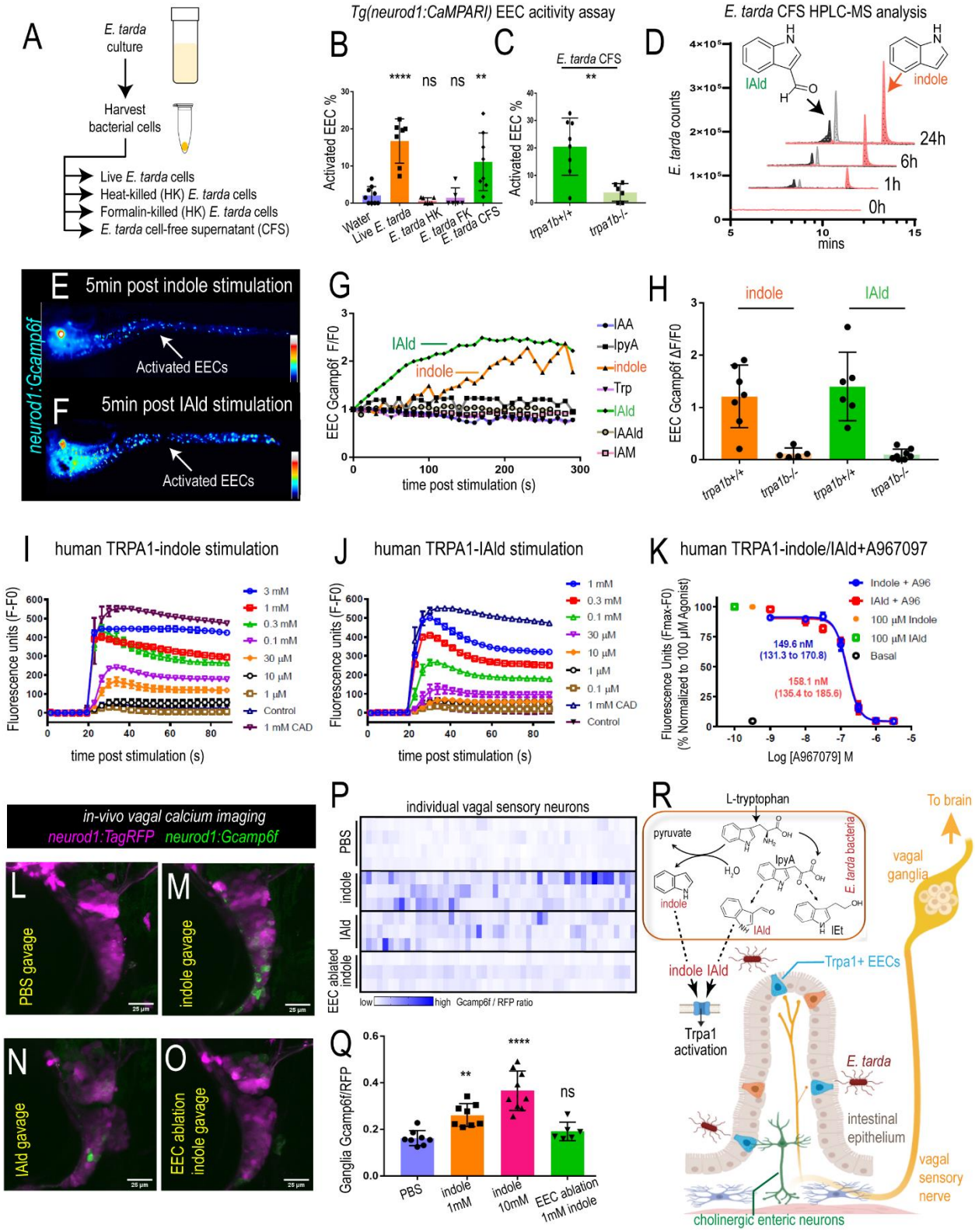

Figure 7. *E. tarda* derived Tryptophan catabolites activate Trpa1 and the EEC-vagal pathway.

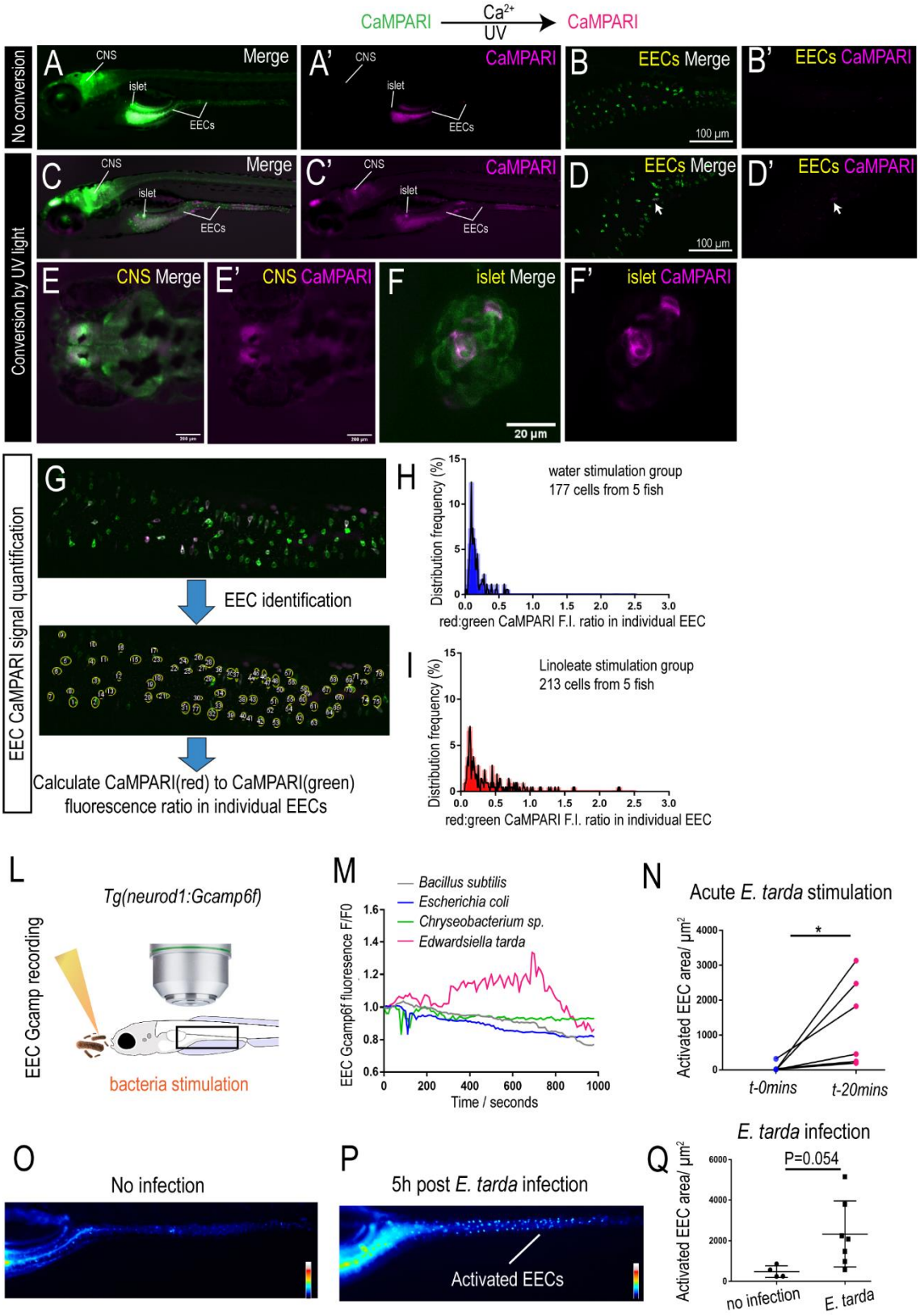

Figure S1. *E. tarda* activates EECs *in vivo*.

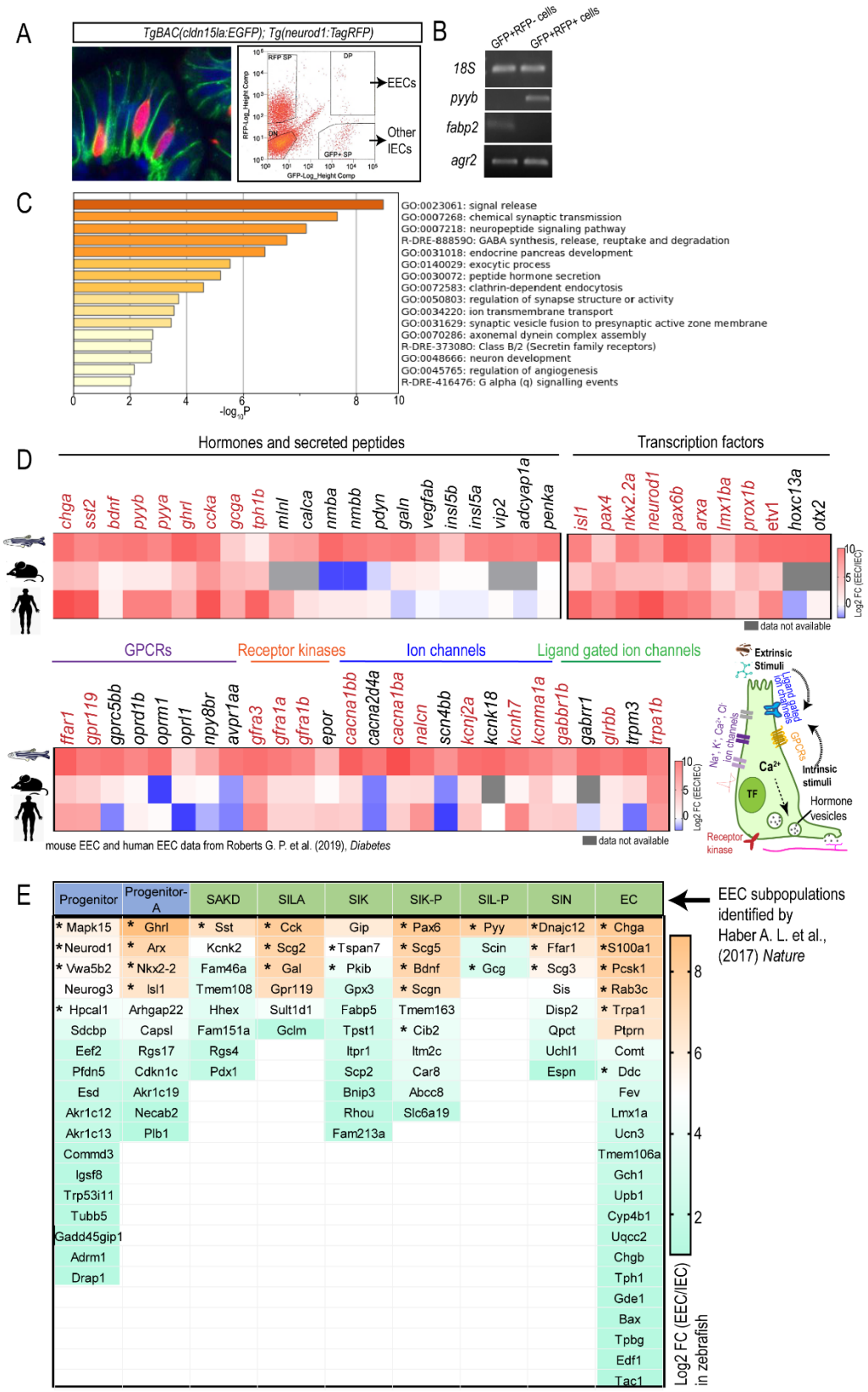

Figure S2. Conserved genetic features between zebrafish and mammalian EECs.

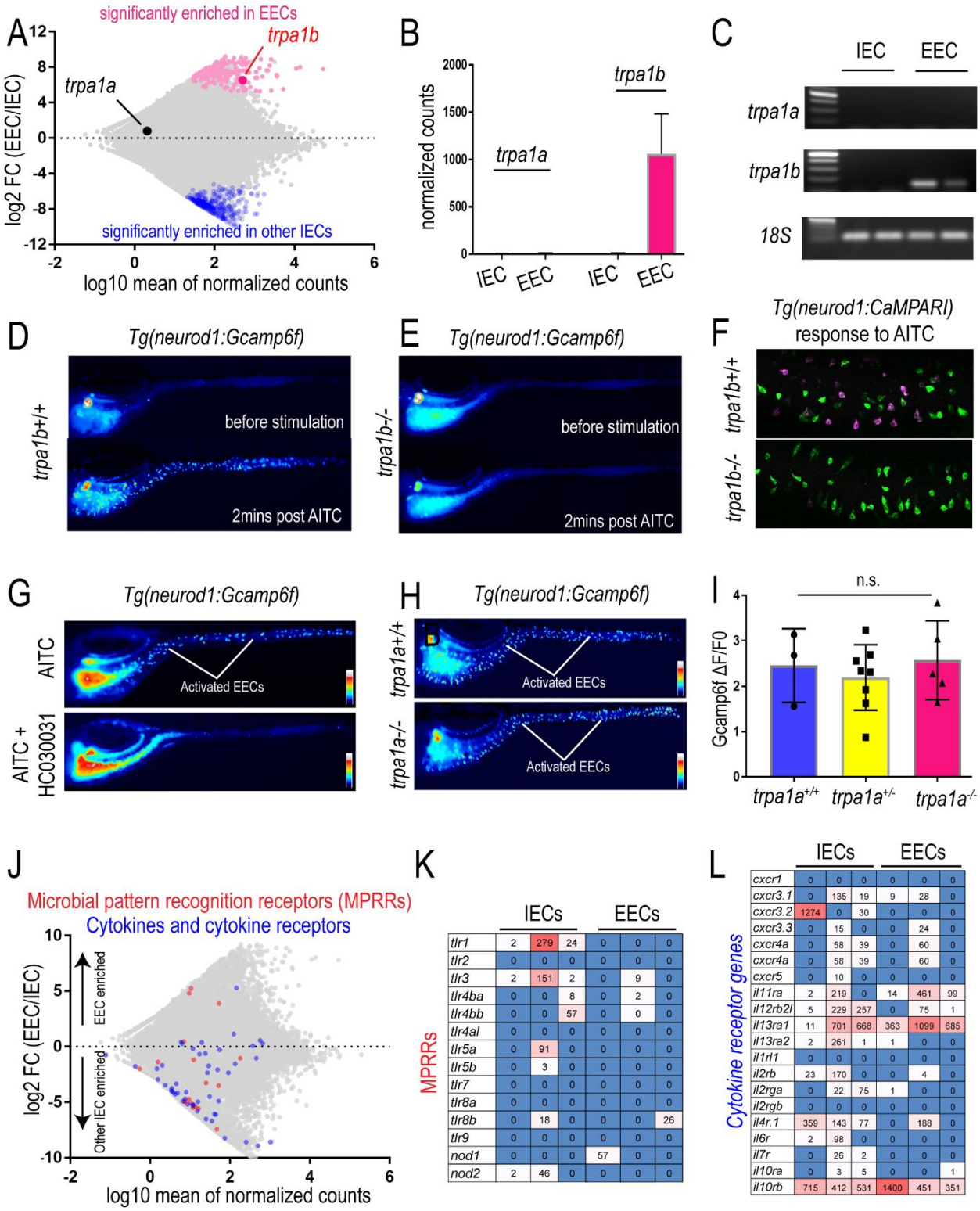

Figure S3. EECs express *trpa1b* and respond to Trpa1 agonist.

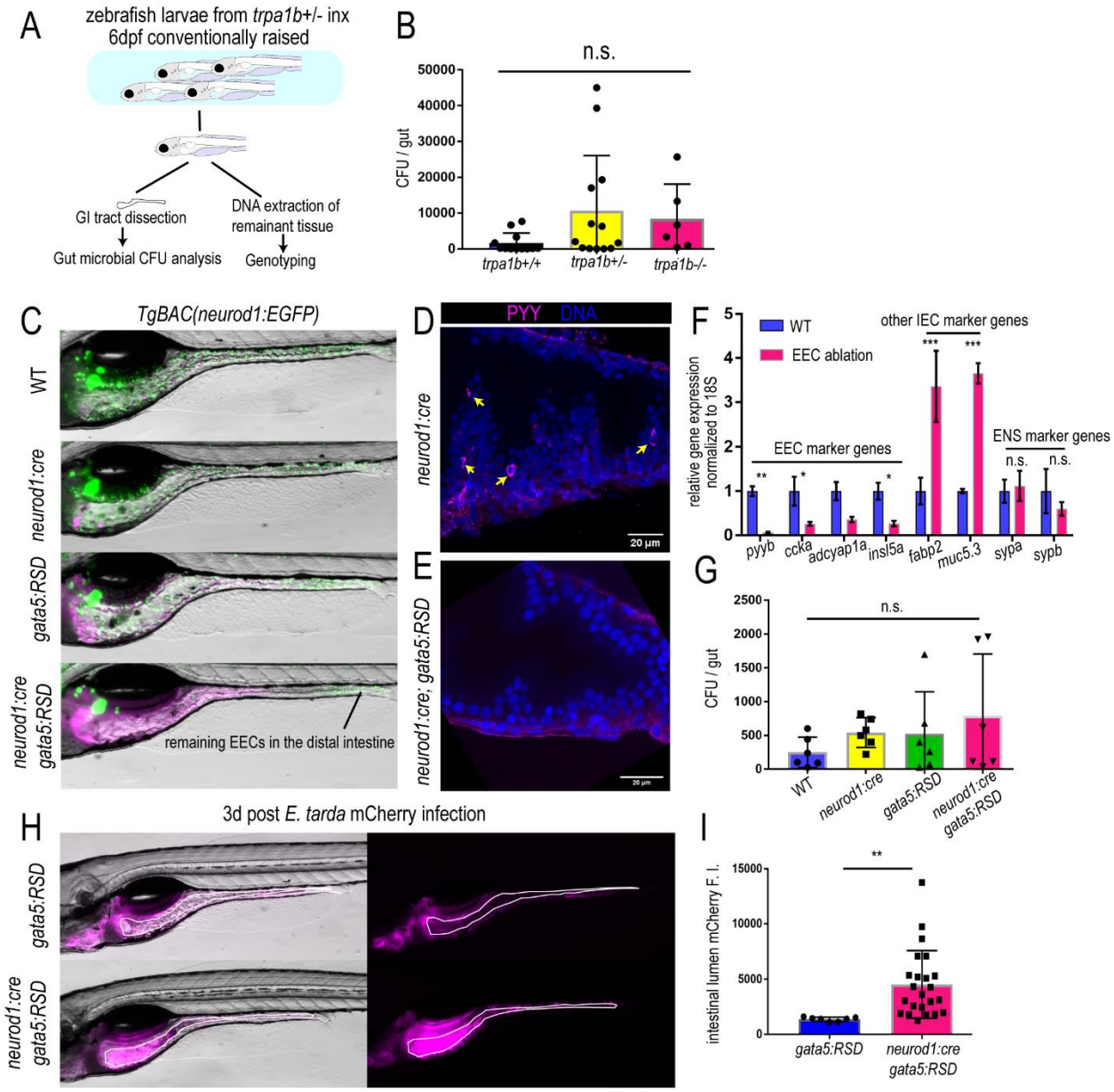

Figure S4. The effects of *trpa1b* and EEC ablation on gut bacterial burden in the conventionalized or *E. tarda*-treated state.

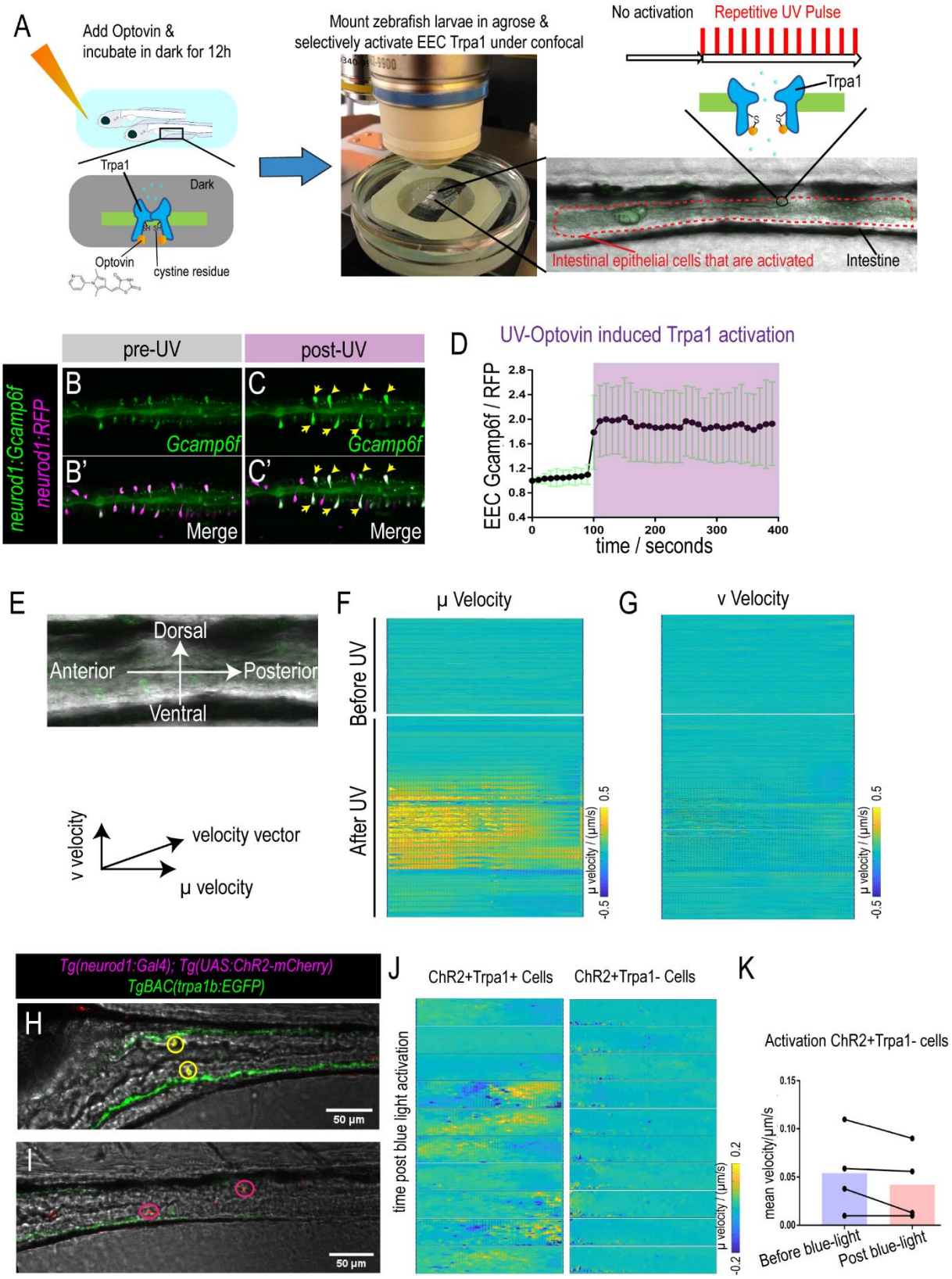

Figure S5. Activation of EEC Trpa1 signaling promotes intestinal motility.

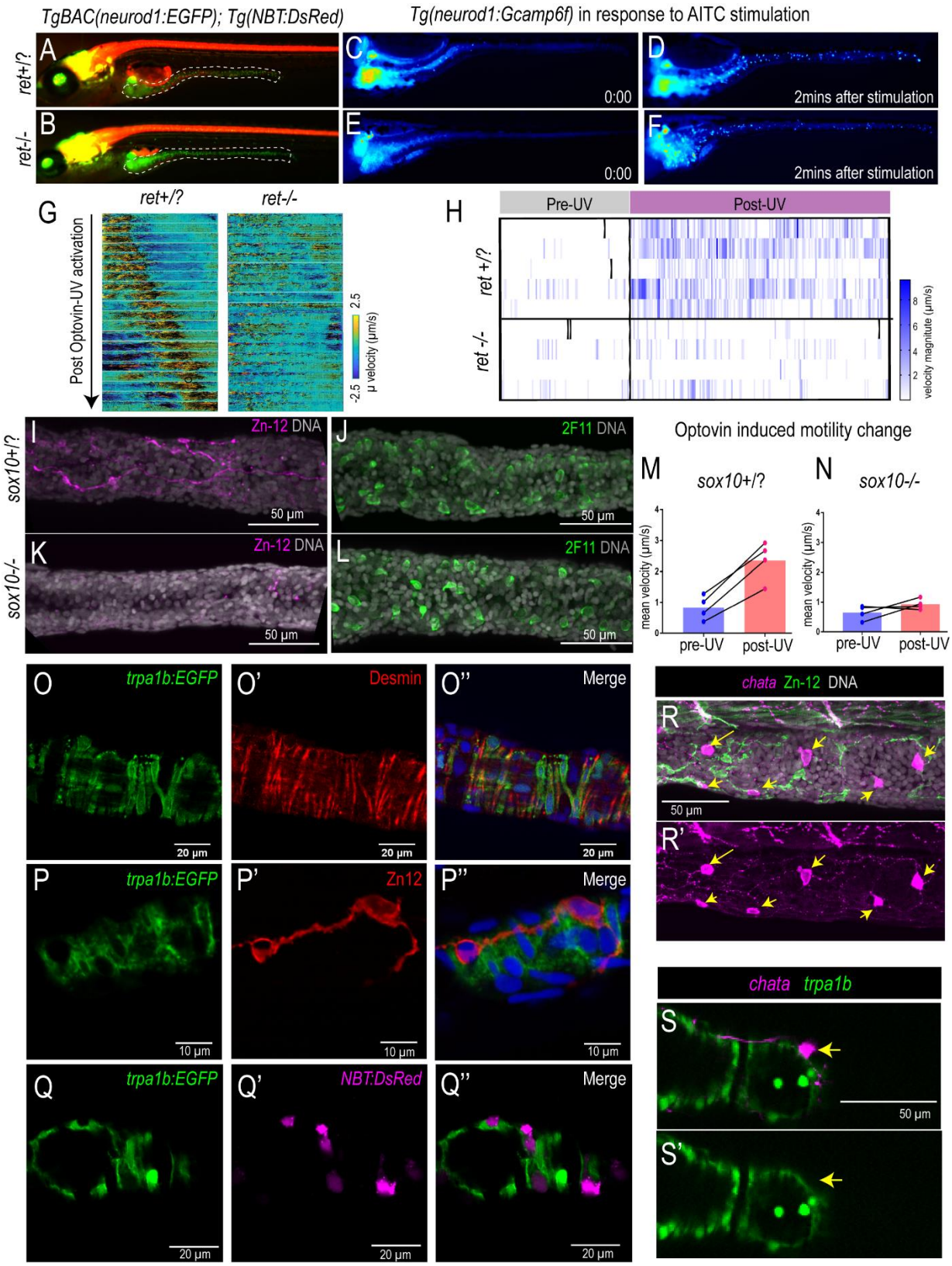

Figure S6. The enteric nervous system in EEC Trpa1-induced intestinal motility.

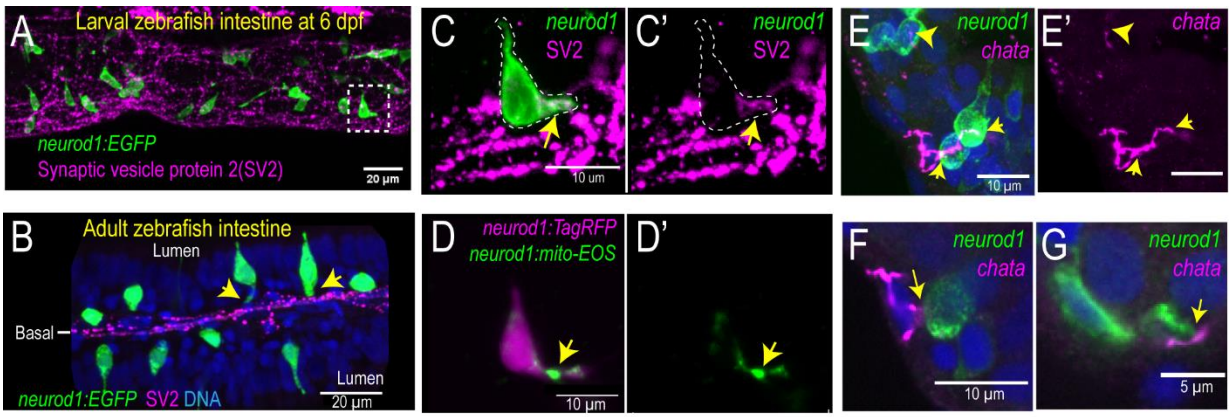

H

pcloa	8.91	3.51	3.67
pclob	7.78	3.51	3.67
bsnb	7.10	0.11	6.78
rims2a	6.34	2.55	7.38
nsfa	2.30	0.26	0.99
syngr3a	4.15	0.03	1.32
syngr3b	6.87	0.03	1.32
syt1a	8.54	-0.32	-0.32
syt4	8.33	-0.25	5.09
syt11a	5.50	1.17	3.02
syt17	6.56	1.93	4.25
syt6a	7.31	NA	1.19
scg5	7.61	3.32	8.49
scg2b	7.62	5.31	9.58
scgn	6.82	3.96	9.01
scg3	5.52	3.38	7.20
scg2a	5.37	5.31	9.58
stx1b	7.60	0.27	0.30
munc18a	7.86	2.40	4.48
vamp2	5.65	2.28	0.93
nrxn1a	3.95	0.75	1.31
nrxn1b	6.75	0.75	1.31
cplx2	2.13	3.75	7.35
snap25a	6.82	3.21	8.35

Log2 FC (EEC/IEC)

mouse EEC and human EEC data from Roberts G. P. et al. (2019) *Diabetes*

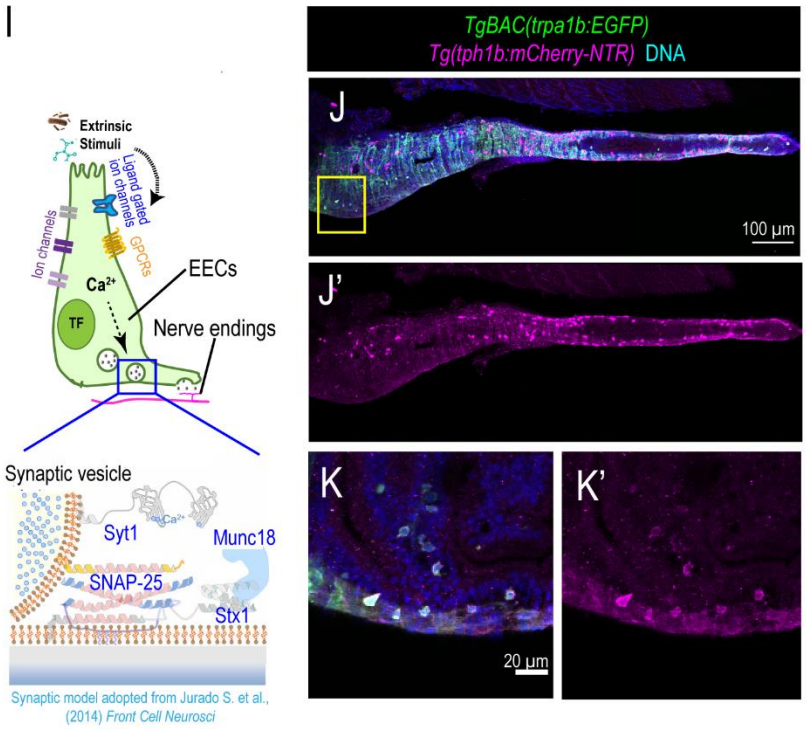

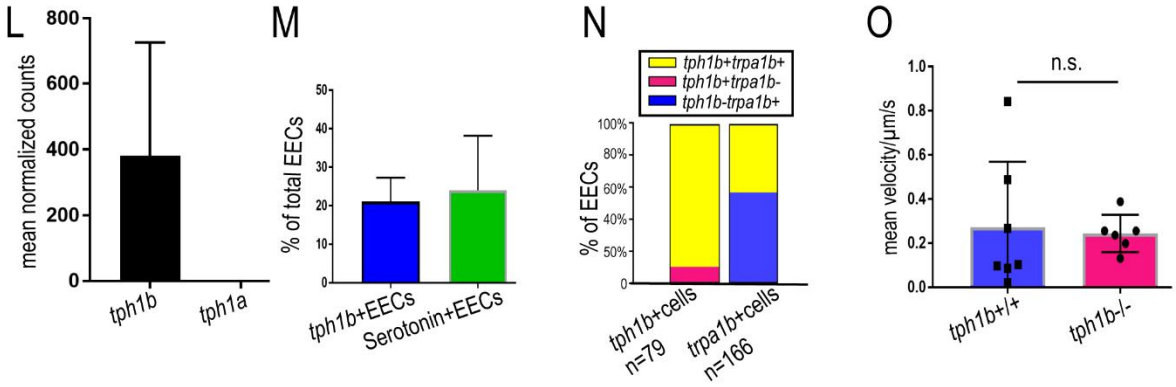

Figure S7. Zebrafish EECs exhibit conserved presynaptic markers and 5-HT expression.

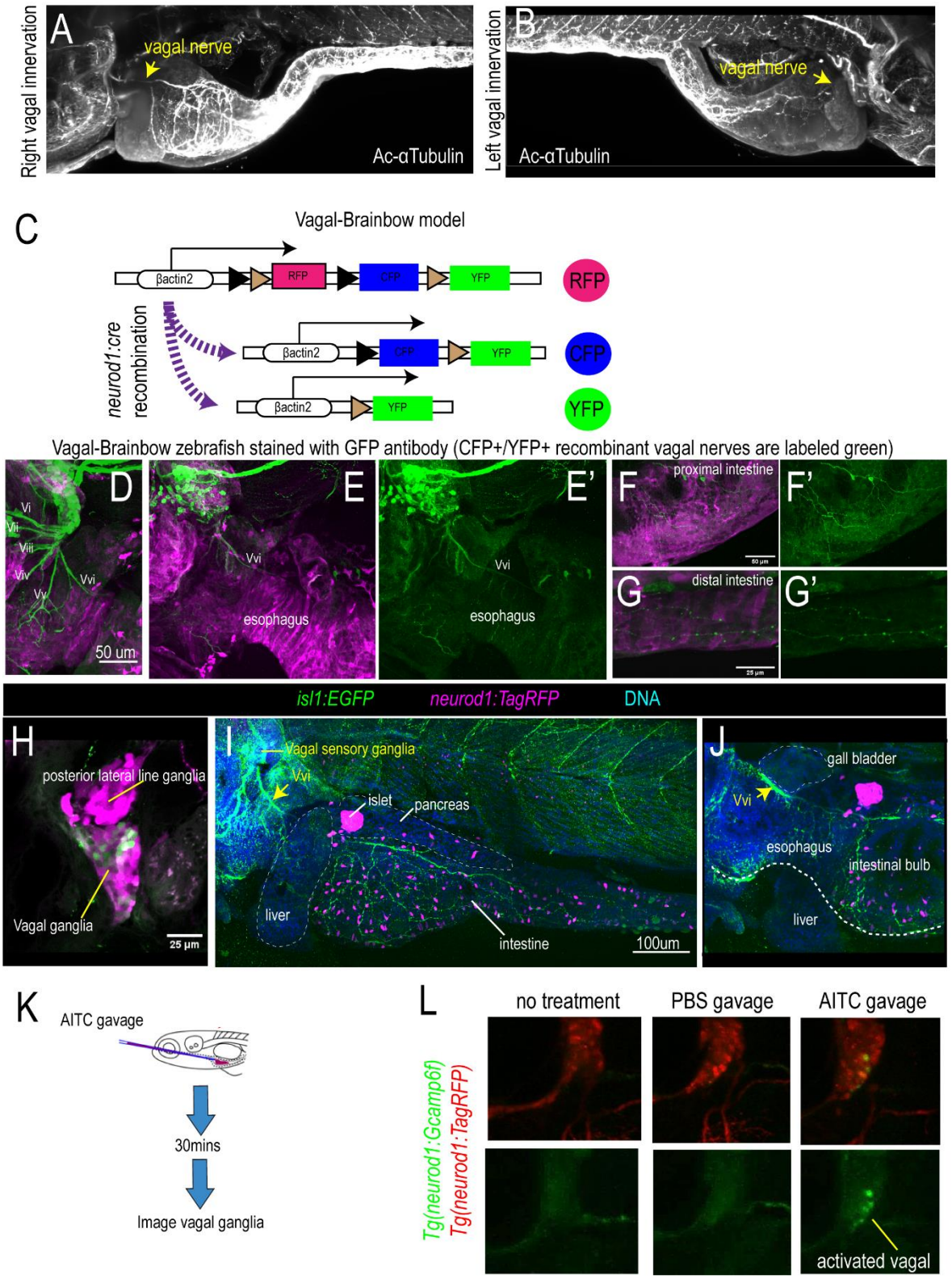

Figure S8. Zebrafish vagal sensory nerve innervate the intestine.

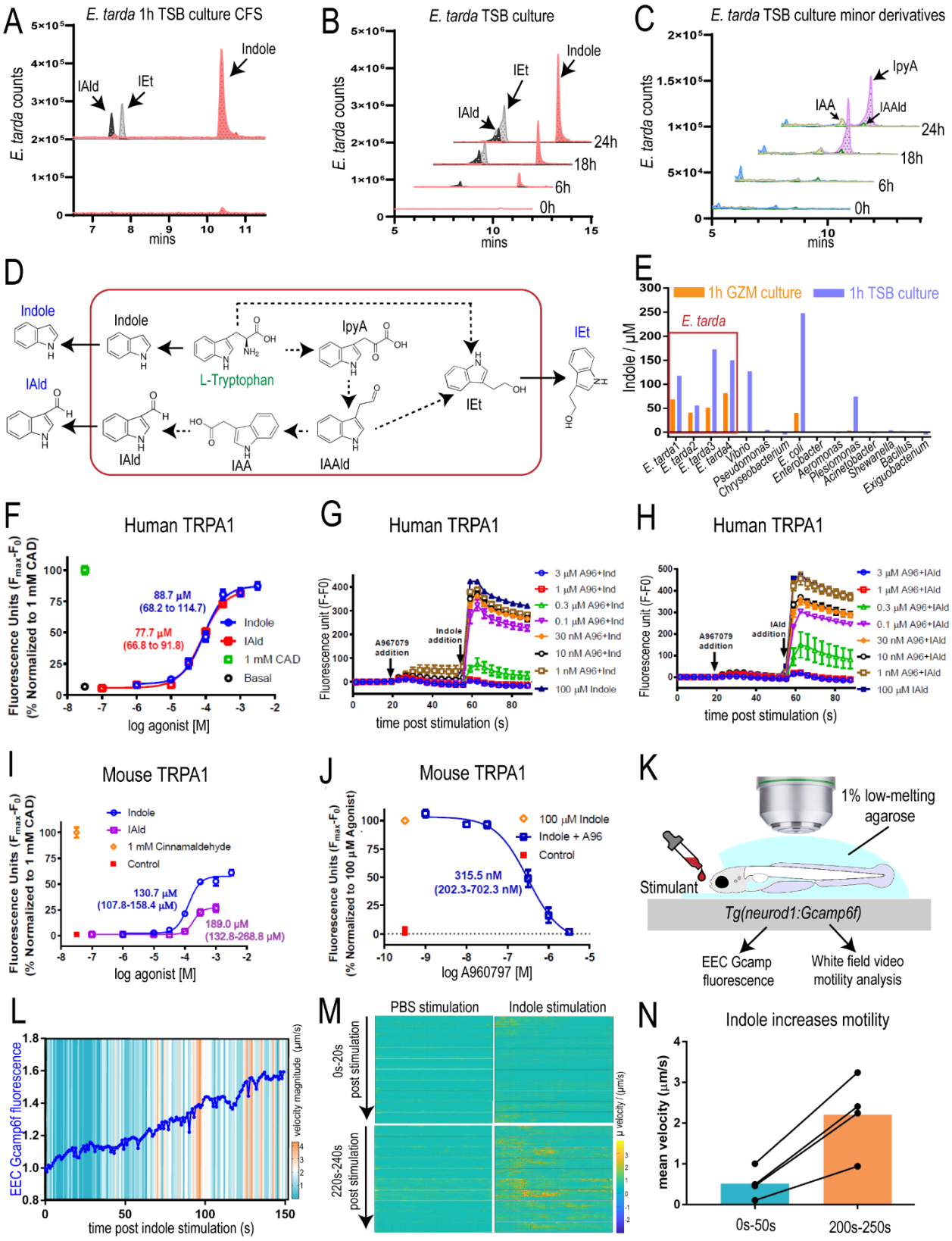

Figure S9. *E. tarda* derived tryptophan catabolites activate Trpa1.

METHODS

Zebrafish strains and husbandry

All zebrafish experiments conformed to the US Public Health Service Policy on Humane Care and Use of Laboratory Animals, using protocol number A115-16-05 approved by the Institutional Animal Care and Use Committee of Duke University. For experiments involving conventionally raised zebrafish larvae, adults were bred naturally in system water and fertilized eggs were transferred to 100mm petri dishes containing ~25 mL of egg water at approximately 6 hours post-fertilization. The resulting larvae were raised under a 14 h light/10 h dark cycle in an air incubator at 28°C at a density of 2 larvae/mL water. All the experiments performed in this study ended at 6 dpf unless specifically indicated. The strains used in this study are listed in Table S1. All lines were maintained on a mixed Ekkwill (EKW) background.

The Gateway Tol2 cloning approach was used to generate the *neurod1:CaMPARI* and *neurod1:cre* plasmids [86, 87]. The 5kb pDONR-neurod1 P5E promoter was previously reported [25] and generously provided by Dr. Hillary McGraw. The pME-cre plasmid as reported previously [88] was generously donated by Dr. Mark Cronan. The pcDNA3-CaMPARI plasmid was reported previously [18] and obtained from Addgene. The CaMPARI gene was cloned into pDONR-221 plasmid using BP clonase (Invitrogen, 11789-020) to generate PME-CaMPARI. pDONR-neurod1 P5E and PME-CaMPARI were cloned into pDestTol2pA2 using LR Clonase (ThermoFisher,11791). Similarly, pDONR-neurod1 P5E and pME-cre were cloned into pDestTol2CG2 containing a cmlc2:EGFP marker. The final plasmid was sequenced and injected into the wild-type EKW zebrafish strain and the F2 generation of alleles *Tg(neurod1:CaMPARI)*^{rdu78} and *Tg(neurod1:cre; cmlcl2:EGFP)*^{rdu79} were used for this study.

To generate the *TgBAC(gata5:loxp-mCherry-stop-loxp-DTA)* transgenic line, the translational start codon of *gata5* in the BAC clone DKEYP-73A2 was replaced with the loxP-mCherry-STOP-loxP-DTA (RSD) cassette by Red/ET recombineering technology (GeneBridges). For recombination with arms flanking the RSD cassette, the 5' homologous arm used was a 716 bp fragment upstream of the start codon and the 3' homologous arm was a 517 bp downstream fragment. The vector-derived loxP site was replaced with an I-SceI site using the same technology. The final BAC was purified using the Qiagen Midipre kit, and coinjected with I-SceI into one-cell stage zebrafish embryos. The full name of this transgenic line is *Tg(gata5:loxP-mCherry-STOP-loxP-DTA)*^{pd315}.

Tg(tph1b:mCherry-NTR)^{pd275} zebrafish were generated using I-SceI transgenesis in an Ekkwill (EK) background. Golden Gate Cloning with BsaI-HF restriction enzyme (NEB) and T4 DNA ligase (NEB) was used to generate the tph1b:mCherry-NTR plasmid by cloning the 5kb *tph1b* promoter sequence (tph1bP GG F: GGTCTCGATCGGtctaaggtgaatctgtcacattc; tph1bP GG R: GGTCTCGGCTACggatggatgctcttgttttatag), mCherry (mC GG F: GGTCTCGTAGCC gccgccaccatggtgag; mC GG2 R: GGTCTCGGTACCcttgtacagctcgtccatgccgcc), a P2A polycistronic sequence and triple mutant variant nitroreductase [89] (mutNTR GG F: GGTCTCGGTACCtacttgtacaagggaagcggagc; mutNTR GG2 R: GGTCTCCCATGC caggatcggtcgtgctcga), into a pENT7 vector backbone with a poly-A tail and I-SceI sites (pENT7 mCN GG F: GGTCTCGCATGGacacctccccctgaacctg; pENT7 mCN GG R: GGTCTCCCGATC gtcaaaggtttggggtccgc). 500 pL of 25 ng/μL plasmid, 333 U/mL I-SceI (NEB), 1x I-SceI buffer, 0.05% Phenol Red (Sigma-Aldrich) solution was injected into EK 1-cell zebrafish embryos. F0 founders were discovered by screening for fluorescence in outcrossed F1 embryos.

RNA sequencing and bioinformatic analysis

Conventionalized (CV) and germ-free (GF) *TgBAC(cldn15la:EGFP); Tg(neurod1:TagRFP)* ZM000 fed zebrafish larvae were derived and reared using our published protocol [90] for Flow Activated Cell Sorting (FACS) to isolate zebrafish EECs and other IECs. The protocol for FACS was adopted from a previous publication [91]. Replicate pools of 50-100 double transgenic *TgBAC(cldn15la:EGFP); Tg(neurod1:TagRPF)* zebrafish larvae were euthanized with Tricaine and washed with deyolking buffer (55 mM NaCl, 1.8 mM KCl and 1.25 mM $NaHCO_3$) before they were transferred to dissociation buffer [HBSS supplemented with 5% heat-inactivated fetal bovine serum (HI-FBS, Sigma, F2442) and 10 mM HEPES (Gibco, 15630–080)]. Larvae were dissociated using a combination of enzymatic disruption using Liberase (Roche, 05 401 119 001, 5 µg/mL final), DNaseI (Sigma, D4513, 2 µg/mL final), Hyaluronidase (Sigma, H3506, 6 U/mL final) and Collagenase XI (Sigma, C7657, 12.5 U/mL final) and mechanical disruption using a gentleMACS dissociator (Miltenyi Biotec, 130-093-235). 400 µL of ice-cold 120 mM EDTA (in 1x PBS) wwas added to each sample at the end of the dissociation process to stop the enzymatic digestion. Following addition of 10 mL Buffer 2 [HBSS supplemented with 5% HI-FBS, 10 mM HEPES and 2 mM EDTA], samples were filtered through 30 µm cell strainers (Miltenyi Biotec, 130-098-458). Samples were then centrifuged at 1800 rcf for 15 minutes at room temperature. The supernatant was decanted, and cell pellets were resuspended in 500 µL Buffer 2. FACS was performed with a MoFlo XDP cell sorter (Beckman Coulter) at the Duke Cancer Institute Flow Cytometry Shared Resource. Single-color control samples were used for compensation and gating. Viable EECs or IECs were identified as 7-AAD negative.

Samples from three independent experimental replicates were performed. 250-580 EECs (n=3 for each CV and GF group) and 100 IECs (n=3 for each CV and GF group) from each experiment were used for library generation and RNA sequencing. Total RNA was extracted from cell pellets using the Argencourt RNAdvance Cell V2 kit (Beckman) following the manufacturer's instructions. RNA amplification prior to library preparation had to be performed. The Clontech SMART-Seq v4 Ultra Low Input RNA Kit (Takara) was used to generate full-length cDNA. mRNA transcripts were converted into cDNA through Clontech's oligo(dT)-priming method. Full length cDNA was then converted into an Illumina sequencing library using the Kapa Hyper Prep kit (Roche). In brief, cDNA was sheared using a Covaris instrument to produce fragments of about 300 bp in length. Illumina sequencing adapters were then ligated to both ends of the 300bp fragments prior to final library amplification. Each library was uniquely indexed allowing for multiple samples to be pooled and sequenced on two lanes of an Illumina HiSeq 4000 flow cell. Each HiSeq 4000 lane could generate >330M 50bp single end reads per lane. This pooling strategy generated enough sequencing depth (~55M reads per sample) for estimating differential expression. Sample preparation and sequencing was performed at the GCB Sequencing and Genomic Technologies Shared Resource.

Zebrafish RNA-seq reads were mapped to the danRer10 genome using HISAT2(Galaxy Version 2.0.5.1) using default settings. Normalized counts and pairwise differentiation analysis were carried out via DESeq2 [92] with the web based-galaxy platform: https://usegalaxy.org/. For the purpose of this study, we only displayed the CV EEC (n=3) and CV IEC (n=3) comparison and analysis in the Results section. The default significance threshold of FDR < 5% was used for comparison. Hierarchical clustering of replicates and a gene expression heat map of RNA-seq data were generated using the online expression heatmap tool: http://heatmapper.ca/expression/. The human and mouse RNA-seq raw counts data were obtained from the NCBI GEO repository:

human, GSE114853; mouse, GSE114913 [26]. Pairwise differentiation analysis of human jejunum CHGA+ (n=11) and CHGA- (n=11) and mouse duodenum Neurod1+ (n=3) and Neurod1- (n=3) was performed using DESeq2. The mouse and zebrafish ortholog Gene ID conversion was downloaded from Ensemble. The genes that were significantly enriched (P_{FDR}<0.05) in the human and mouse EEC data sets were used to query the zebrafish EEC RNA seq dataset and data were plotted using Graphpad Prism7. RNA-seq data generated in this study can be accessed at GSE151711.

Recording *in vivo* EEC activity

CaMPARI undergoes permanent green-to-red photoconversion (PC) under 405 nm light when calcium is present. This permanent conversion records the calcium activity for all areas illuminated by PC-light. Red fluorescence intensity correlates with calcium activity during photoconversion [18]. To record *in vivo* EEC activity using the CaMPARI platform, conventionally raised *Tg(neurod1:CaMPARI)* zebrafish larvae were sorted at 3 dpf and maintained in Gnotobiotic Zebrafish Media (GZM) [90] with 1 larvae/mL density. At 6 dpf, for each experimental group, ~20 larvae were transferred into 50mL conical tubes in 2 mL GZM medium. The larvae were adjusted to the new environment for 30 mins before stimuli were added to each conical tube. For nutrient stimulation, since linoleate, oleate and laurate are not soluble in water, a bovine serum albumin (BSA) conjugated fatty acid solution was generated as described previously [6]. 2 mL linoleate, oleate, laurate, butyrate or glucose was added to the testing tube containing ~20 zebrafish larvae in 3 mL GZM. The final stimulant concentrations were: linoleate (1.66 mM), oleate oleate (1.66 mM), laurate (1.66 mM), butyrate (2 mM) and glucose (500 mM). Zebrafish larvae were stimulated for 2 mins (fatty acids) or 5 mins (glucose) before the UV pulse. For bacterial stimulation, single colonies of the different bacterial strains were cultured aerobically in tryptic soy broth (TSB) at 30°C overnight (rotating 50-60 rpm, Thermo Fisher Tissue Culture Rotator CEL-GRO #1640Q)(see strains listed in Table S1). ~10^{10} bacteria were harvested, washed with GZM and resuspended in 2 mL GZM. 2 mL bacteria were then added to a test tube containing ~20 zebrafish larvae in 3 mL GZM. Zebrafish were then stimulated for 20mins before treated with a UV pulse. A customized LED light source (400 nm-405 nm, Hongke Lighting CO. LTD) was used to deliver a UV light pulse (100 W power, DC32-34 V and 3500 mA) for 30 seconds. Following the UV pulse, zebrafish larvae were transferred to 6-well plates. To block spontaneous intestinal motility and facilitate *in vivo* imaging, zebrafish larvae were incubated in 20 µM 4-DAMP (mAChR blocker), 10 µM atropine (mAChR blocker) and 20 µM clozapine (5-HTR blocker) for 30 mins. Zebrafish larvae were then anesthetized with Tricaine (1.64 mg/ml) and mounted in 1% low melting agarose and imaged using a 780 Zeiss upright confocal microscope in the Duke Light Microscope Core Facility. Z-stack confocal images were taken of the mid-intestinal region in individual zebrafish. The laser intensity and gain were set to be consistent across different experimental groups. The resulting images were then processed and analyzed using FIJI software [93]. To quantify the number of activated EECs, the color threshold was set for the CaMPARI red channel. EECs surpassing the color threshold were counted as activated EECs. The CaMPARI green channel was used to quantify the total number of EECs in each sample. The ratio of activated EECs to the total EEC number was calculated as the percentage of activated EECs.

To record *in vivo* EEC activity using the *Tg(neurod1:Gcamp6f)* system, we used our published protocol with slight modification [6]. In brief, unanesthetized zebrafish larvae were gently mounted in 3% methylcellulose. Excess water was removed and zebrafish larvae were gently positioned with right side up. Zebrafish were then moved onto an upright Leica M205 FA fluorescence

stereomicroscope equipped with a Leica DFC 365FX camera. The zebrafish larvae were allowed to recover for 2mins before 100 µL of test agent was pipetted directly in front of the mouth region. Images were then recorded every 10 seconds. The stimulants used in this study are listed in Supplemental Table 1. The data shown in Fig. 2O-R, depicting the EEC responses to *E. tarda* stimulation, were obtained by mounting unanesthetized zebrafish larvae in 1% low melting agarose. A window (5 × 5 mm) was cut to expose the head region of the zebrafish. 10 µL of *E. tarda* culture [~10^9 Colony Forming Unit (CFU)] were delivered at the zebrafish mouth area. Images were recorded every 10 secs for 20 mins. Image processing and analysis were performed using FIJI software. Time-lapse fluorescence images were first aligned to correct for experimental drift using the plugin "align slices in stack." Normalized correlation coefficient matching and bilinear interpolation methods for subpixel translation were used for aligning slices [94]. The plugin "rolling ball background subtraction" with the rolling ball radius=10 pixels was used to remove the large spatial variation of background intensities. The Gcamp6f fluorescence intensity in the intestinal region was then calculated for each time point. The ratio of maximum fluorescence (Fmax) and the initial fluorescence (F0) was used to measure EEC calcium responses.

Immunofluorescence staining and imaging

Whole mount immunofluorescence staining was performed as previously described [6]. In brief, ice cold 2.5% formalin was used to fix zebrafish larvae overnight at 4°C. The samples were then washed with PT solution (PBS+0.75%Triton-100). The skin and remaining yolk were then removed using forceps under a dissecting microscope. The deyolked samples were then permeabilized with methanol for more than 2 hrs at -20°C. Samples were then blocked with 4% BSA at room temperature for more than 1 hr. The primary antibody was diluted in PT solution and incubated at 4°C for more than 24 hrs. Following primary antibody incubation, the samples were washed with PT solution and incubated overnight with secondary antibody with Hoechst 33342 for DNA staining. Imaging was performed with Zeiss 780 inverted confocal and Zeiss 710 inverted confocal microscopes with 40× oil lens. The primary antibodies were listed in Supplemental Table 1. The secondary antibodies in this study were from Alexa Fluor Invitrogen were used at a dilution of 1:250.

To quantify vagal activity by pERK staining, we used a published protocol with slight modification [50]. Zebrafish larvae were quickly collected by funneling through a 0.75 mm cell strainer and dropped into a 5mL petri dish containing ice cold fix buffer (2.5% formalin+ 0.25% Triton 100). Larvae were fixed overnight at 4°C, then washed 3 times in PT (PBS+ 0.3% Triton 100), treated with 150 mM Tris-HCl (PH=9) for 15 mins at 70°C, washed with PT and digested with 0.05% trypsin-EDTA on ice for 45 mins. Following digestion, samples were then washed with PT and transferred into block solution [PT + 1% bovine serum albumin (BSA, Fisher) + 2% normal goat serum (NGS, Sigma) + 1% dimethyl sulfoxide (DMSO)]. The primary antibodies [pERK (Cell signaling); tERK (Cell signaling); GFP (Aves Lab)] were diluted in block solution (1:150 for pERK; 1:150 for tERK and 1:500 for GFP) and samples were incubated in 100 µl of primary antibody overnight at 4°C. Following primary antibody incubation, samples were then washed with PT and incubated with secondary antibody overnight at 4°C. Samples were then washed with PBS, mounted in 1% LMA and imaged using a Zeiss 780 upright confocal microscope.

Zebrafish *E. tarda* colonization

For *E. tarda* colonization experiments, fertilized zebrafish eggs were collected, sorted and transferred into a cell culture flask containing 80 mL GZM at 0 dpf. At 3 dpf, dead embryos and

60 mL GZM were removed and replaced with 50 mL fresh GZM in each flask. To facilitate consistent commensal gut bacterial colonization, an additional 10 mL of filtered system water (5 µm filter, SLSV025LS, Millipore) were added to each flask. Overnight *E. tarda* mCherry (Amp^r, see details in Supplemental Table 1) culture was harvested, washed three times with GZM. 150 µL of GZM-washed *E. tarda* mCherry culture were inoculated into each flask. Daily water changes (60 ml) was performed and 200 µL autoclaved solution of ZM000 food (ZM Ltd.) was added from 3 dpf to 6 dpf as previously described [90]. At 6 dpf, zebrafish larvae were subjected to fluorescence imaging analysis or CFU quantification. For fluorescence imaging analysis, zebrafish larvae were anesthetized with Tricaine (1.64 mg/ml), mounted in 3% methylcellulose and imaged with a Leica M205 FA upright fluorescence stereomicroscope equipped with a Leica DFC 365FX camera. For CFU quantification, digestive tracts were dissected and transferred into 1 mL sterile PBS which was then mechanically disassociated using a Tissue-Tearor (BioSpec Products, 985370). 100 µL of serially diluted solution was then spread on a Tryptic soy agar (TSA) plate with Carbenicillin (100 µg/ml) and cultured overnight at 30°C under aerobic conditions. The mCherry+ colonies were quantified from each plate and *E. tarda* colony forming units (CFUs) per fish were calculated.

Optic EEC activation

For EEC Trpa1 activation using the Optovin platform, zebrafish larvae were treated with 10 µM Optovin overnight. Following Optovin treatment, zebrafish were mounted in 1% LMA and imaged under a 780 upright Zeiss confocal microscope using 20× water objective lenses. For all the experiments, the mid-intestine region was imaged (Fig. S5A). The intestinal epithelium was selected as the region of interest (ROI) (Fig. S5A). Serial images were obtained at 1 s/frame. A 405 nm pulse of light was applied to the ROI at 1 pulse/10s. For some experiments (Fig. 4D-F, Fig. S5B-G), the images were obtained at 10s/frame. When measuring Optovin effects on intestinal motility in *ret-/-*, *sox10-/-* or *tph1b-/-* zebrafish larvae, embryos were collected from heterozygous zebrafish. *ret-/-* zebrafish were identified by lack of ENS and deflated swim bladder [95], *sox10-/-* zebrafish were identified by lack of pigment [96], and *tph1b-/-* zebrafish were identified by PCR-based genotyping [47].

Photoactivation of channelrhodopsin (ChR2) in EECs was performed in *Tg(neurod1:Gal4, cmlc2;EGFP); Tg(UAS:ChR2-mCherry)* transgenic zebrafish. In this model, ChR2 expression in EECs is mosaic. At 6 dpf, unanesthetized zebrafish larvae were mounted in 1% LMA. Photoactivation and imaging were performed with a Zeiss 780 upright confocal using 20× water objective lenses. Individual ChR2+ EECs were selected as ROI (Fig. S5H, I). Serial images were obtained at 1 s/frame. The 488 nm and 458 nm pulses were applied to the selected ROI at 1 pulse/s. For selectively activating *trpa1b*+ or *trpa1b*- ChR2 expressing EECs, *Tg(neurod1:Gal4, cmlc2;EGFP); Tg(UAS:ChR2-mCherry)* was crossed with *TgBAC(trpa1b:EGFP)*. A snapshot of the intestinal area was obtained to determine the *trpa1b*+ChR2+ and *trpa1b*-ChR2+ EECs (Fig. S5H, I) and light pulses were applied to the selected EECs as indicated above.

To determine whether Optovin-UV or ChR2 was sufficient to activate EECs, *Tg(neurod1:Gcamp6f)* zebrafish were used. To facilitate EEC calcium imaging under the confocal microscope, zebrafish larvae were incubated in 20 µM 4-DAMP, 10 µM atropine and 20 µM clozapine for 30 mins before mounting in 1% LMA to reduce spontaneous motility. The Gcamp6f signal was recorded with 488nm laser intensity less than 0.5.

The zebrafish intestinal motility is quantified through recorded image series of zebrafish intestine using the method similar as previously described [97]. Intestinal μ velocity, v velocity and μ velocity magnitude were used to estimate intestinal motility in zebrafish as previously described using the PIV-Lab MATLAB app [97]. The MTrackJ FIJI plugin was used to quantify the mean velocity magnitude [98].

Enteric cholinergic neuron and vagal ganglion calcium imaging

TgBAC(chata:Gal4); Tg(UAS:Gcamp6s); Tg(NBT:DsRed) zebrafish were used to record *in vivo* calcium activity in enteric cholinergic neurons. The NBT promoter labels all ENS neurons while the Chata promoter labels only cholinergic enteric neurons. DsRed fluorescence was used as reference for cholinergic neuron Gcamp quantification. Zebrafish larvae were incubated in 20 μM 4-DAMP and 20 μM clozapine for 30 mins before mounting in 1% LMA to reduce spontaneous motility and facilitate *in vivo* imaging using a Zeiss 780 upright confocal microscope with 20× water lenses. Serial images were taken at 5 s/frame. To record cholinergic neuron calcium activation, zebrafish was pretreated with Optovin and 40 nm light was applied at the frequency of 1 pulse/5s to the intestinal epithelium ROI. The Gcamp6s to DsRed fluorescence in cholinergic neurons was calculated for recorded.

Tg(neurod1:Gcamp6f); Tg(neurod1:TagRPF) zebrafish were used to record vagal sensory ganglia calcium activity *in vivo*. Zebrafish were anesthetized with 1 mg/mL α-Bungarotoxin (α-BTX) and gavaged with chemical compounds or bacteria as described [99]. Zebrafish larvae were mounted in 1% LMA and imaged under a Zeiss 780 upright confocal microscope. Z-stack images of the entire vagal ganglia were collected as serial images at 10 mins/frame and processed in FIJI. Individual vagal sensory neurons were identified and the Gcamp6f to TagRFP fluorescence ratios of individual vagal sensory neurons were calculated.

Quantitative real-time PCR

Quantitative real-time PCR was performed as described previously [100]. In brief, 20 zebrafish larvae digestive tracts were dissected and pooled into 1 mL TRIzol (ThermoFisher, 15596026). mRNA was then isolated with isopropanol precipitation and washed with 70% ethanol. 500ng mRNA was used for cDNA synthesis using the iScript kit (Bio-Rad, 1708891). Quantitative PCR was performed in triplicate 25 μL reactions using 2X SYBR Green SuperMix (PerfeCTa, Hi Rox, Quanta Biosciences, 95055) run on an ABI Step One Plus qPCR instrument using gene specific primers (Supplementary file 1). Data were analyzed with the ΔΔCt method. *18S* was used as a housekeeping gene to normalize gene expression.

Mammalian TRPA1 activity analysis

HEK-293T cells were cultured in DMEM (Thermofisher Scientific, Waltham, MA) and supplemented with 10% fetal bovine serum (FBS) (Thermofisher Scientific), penicillin (100 units/mL) and streptomycin (0.1 mg/mL). Cells were plated on 100 mm tissue culture plates coated with poly-D-lysine (Sigma Aldrich, Saint Louis, MO) and grown to ~60% confluence. The cells were transiently transfected for 16-24 hours with either human or mouse orthologs of TRPA1 using Fugene 6 transfection reagents and Opti-MEM (Thermofisher Scientific) according to the manufacturer's protocol. Subsequently, cells were trypsinized, re-suspended and re-plated onto poly-D-lysine coated 96-well plates (Krystal black walled plates, Genesee Scientific) at $5x10^5$ cells/mL (100 μL/well) and allowed to grow for another 16-20 hrs prior to the experiments. Cells were maintained as monolayers in a 5% CO_2 incubator at 37°C.

Measurements of changes in intracellular Ca^{2+} concentrations ($[Ca^{2+}]_i$) were performed as described previously [101]. In brief, cells in 96-well plates were loaded with Calcium 6, a no-wash fluorescent indicator, for 1.5 hrs (Molecular Devices, San Jose, CA) and then transferred to a FlexStation III benchtop scanning fluorometer chamber (Molecular Devices). Fluorescence measurements in the FlexStation were performed at 37°C (Ex:485 nm, Em: 525 nm at every 1.8 s). After recording baseline fluorescence, agonists (indole, IAld, cinnamaldehyde) were added and fluorescence was monitored for a total of 60 s. To determine the effects of TRPA1 inhibition on agonist response, TRPA1 transfected HEK-293 cells were pretreated with various concentrations of A967079 (Medchem101, Plymouth Meeting, PA), a specific antagonist of TRPA1, and then exposed to either 100 µM indole or IAld. The change in fluorescence was measured as Fmax-F0, where Fmax is the maximum fluorescence and F0 is the baseline fluorescence measured in each well. The EC50 and IC50 values and associated 95% confidence intervals for agonist (Indole and IAld) stimulation of Ca^{2+} influx and A967079 inhibition of agonist-induced Ca^{2+} influx, respectively, were determined by non-linear regression analysis with a 4-parameter logistic equation (Graphpad Prism, San Diego, CA). Indole and IAld concentration-response data was normalized to 1 mM cinnamaldehyde for EC50's calculations and A967079 concentration-response data was normalized to 100 µM indole or IAld for IC50's calculations.

HPLC-MS analysis of Trp-Indole derivatives

The chemical profiling of Trp-Indole derivatives was performed using 1 L culture of *E. tarda*. The strain was inoculated in 3 mL of TSB medium and cultivated for 1 day on a rotary shaker at 180 rpm at 30°C under aerobic conditions. After 1 day, 1 mL of E. tarda liquid culture was inoculated in 1 L of TSB medium in a 4-L Pyrex flask. The *E. tarda* culture was incubated at 30°C for 24 hr under aerobic conditions. For time-course screening, 10 mL from the *E. tarda* TSB culture was collected at 0, 6, 18, and 24 hours. Each 10 mL sample of *E. tarda* culture was extracted with 15 mL of ethyl acetate (EtOAc). The EtOAc layer was separated from the aqueous layer and residual water was removed by addition of anhydrous sodium sulfate. Each EtOAc fraction was dried under reduced pressure, then resuspended in 500 µL of 50% MeOH/50% H_2O and 50 µL of each sample were analyzed using an Agilent Technologies 6130 quadrupole mass spectrometer coupled with an Agilent Technologies 1200–series HPLC (Agilent Technologies, Waldbron, Germany). The chemical screening was performed with a Kinetex® EVO C18 column (100 × 4.6 mm, 5 µm) using the gradient solvent system (10 % ACN/90 % H_2O to 100 % ACN over 20 min at a flow rate of 0.7 mL/min).

For HPLC-MS analysis of *E. tarda* in GZM medium, the remaining 1 L culture of *E. tarda* in TSB culture was centrifuged at 7,000 rpm for 30 min. Pellets were transferred to 1 L of GZM medium in a 4-L Pyrex flask and cultivated on a rotary shaker at 30°C for 24 hr. For time-course screening, 10 mL from the *E. tarda* GZM culture was collected at 0, 1, 6, and 24 hours. Sample preparation and HPLC-MS analysis of *E. tarda* culture GZM medium were performed using same procedures as described above for TSB. Trp-Indole derivatives of *E. tarda* culture broths were identified by comparing the retention time and extracted ion chromatogram with authentic standards. Extracted ions were selected for Indole (m/z 117, Sigma-Aldrich), IAld (m/z 145, Sigma-Aldrich), IAAld (m/z 159, Ambeed), IEt (m/z 161, Sigma-Aldrich), IAM (m/z 174, Sigma-Aldrich), IAA (m/z 175, Sigma-Aldrich), and IpyA (m/z 203, Sigma-Aldrich).

Indole concentration quantification

The indole concentration was measured using the Indole assay kit based on a modified version of Ehlrich's and Kovac's reagents, which reacts with indole to produce a colored compound at 565 nm (Sigma, MAK326). Different bacterial strains were cultured overnight at 30°C in TSB media under aerobic conditions (rotating 50-60rpm, Thermo Fisher Tissue Culture Rotator CEL-GRO #1640Q). ~10^{10} bacteria were harvested, washed with PBS, and resuspended in 5 mL GZM or TSB media. The bacteria culture was then cultured at 30°C (shaking 250 rpm, 1 h) followed by centrifugation and the supernaant was filtered through a 0.22 µm filter. The concentration of indole in the supernatant was measured using a colorimetric kit and plate reader at 565nm absorption (Synergy HTX). 4 *E. tarda* strains and 11 commensal/model bacterial strains were tested. The 4 *E. tarda* strains are: *E. tarda* FL6-60 (*E. tarda1*), *E. tarda* LSE40 (*E. tarda2*), *E. tarda* 23685 (*E. tarda*3) and *E. tarda* 15974 (*E. tarda*4).

Statistical analysis

The appropriate sample size for each experiment was suggested by preliminary experiments evaluating variance and effects. Using significance level of 0.05 and power of 90%, a biological replicate sample number 8 was suggested for EEC CaMPARI analysis. For each experiment, wildtype or indicated transgenic zebrafish embryos were randomly allocated to test groups prior to treatment. Individual data points, mean and standard deviation are plotted in each figure. The raw data points in each figure are represented as solid dots. Data were analyzed using GraphPad Prism 7 software. For experiments comparing just two differentially treated populations, a Student's t-test with equal variance assumptions was used. For experiments measuring a single variable with multiple treatment groups, a single factor ANOVA with post hoc means testing (Tukey) was utilized. Statistical evaluation for each figure was marked * $P<0.05$, ** $P<0.01$, *** $P<0.001$, **** $P<0.0001$ or ns (no significant difference, $P>0.05$).

References:

1. Brown, J.M. and S.L. Hazen, *The gut microbial endocrine organ: bacterially derived signals driving cardiometabolic diseases.* Annu Rev Med, 2015. **66**: p. 343-59.
2. Liu, Y., et al., *Gut Microbial Metabolites of Aromatic Amino Acids as Signals in Host-Microbe Interplay.* Trends Endocrinol Metab, 2020.
3. Medzhitov, R., *Recognition of microorganisms and activation of the immune response.* Nature, 2007. **449**(7164): p. 819-26.
4. Kaiko, G.E. and T.S. Stappenbeck, *Host-microbe interactions shaping the gastrointestinal environment.* Trends Immunol, 2014. **35**(11): p. 538-48.
5. Guo, X., et al., *The Cellular Diversity and Transcription Factor Code of Drosophila Enteroendocrine Cells.* Cell Rep, 2019. **29**(12): p. 4172-4185 e5.
6. Ye, L., et al., *High fat diet induces microbiota-dependent silencing of enteroendocrine cells.* Elife, 2019. **8**.
7. Furness, J.B., et al., *The gut as a sensory organ.* Nat Rev Gastroenterol Hepatol, 2013. **10**(12): p. 729-40.
8. Kaelberer, M.M., et al., *A gut-brain neural circuit for nutrient sensory transduction.* Science, 2018. **361**(6408).
9. Bellono, N.W., et al., *Enterochromaffin Cells Are Gut Chemosensors that Couple to Sensory Neural Pathways.* Cell, 2017. **170**(1): p. 185-198 e16.
10. Symonds, E.L., et al., *Mechanisms of activation of mouse and human enteroendocrine cells by nutrients.* Gut, 2015. **64**(4): p. 618-26.

11. Lu, V.B., F.M. Gribble, and F. Reimann, *Free Fatty Acid Receptors in Enteroendocrine Cells.* Endocrinology, 2018. **159**(7): p. 2826-2835.
12. Chimerel, C., et al., *Bacterial metabolite indole modulates incretin secretion from intestinal enteroendocrine L cells.* Cell Rep, 2014. **9**(4): p. 1202-8.
13. Furness, J.B., W.A. Kunze, and N. Clerc, *Nutrient tasting and signaling mechanisms in the gut. II. The intestine as a sensory organ: neural, endocrine, and immune responses.* Am J Physiol, 1999. **277**(5): p. G922-8.
14. Brookes, S.J., et al., *Extrinsic primary afferent signalling in the gut.* Nat Rev Gastroenterol Hepatol, 2013. **10**(5): p. 286-96.
15. Bautista, D.M., M. Pellegrino, and M. Tsunozaki, *TRPA1: A gatekeeper for inflammation.* Annu Rev Physiol, 2013. **75**: p. 181-200.
16. Lapointe, T.K. and C. Altier, *The role of TRPA1 in visceral inflammation and pain.* Channels (Austin), 2011. **5**(6): p. 525-9.
17. Nilius, B., J. Prenen, and G. Owsianik, *Irritating channels: the case of TRPA1.* J Physiol, 2011. **589**(Pt 7): p. 1543-9.
18. Fosque, B.F., et al., *Neural circuits. Labeling of active neural circuits in vivo with designed calcium integrators.* Science, 2015. **347**(6223): p. 755-60.
19. Rawls, J.F., et al., *Reciprocal gut microbiota transplants from zebrafish and mice to germ-free recipients reveal host habitat selection.* Cell, 2006. **127**(2): p. 423-33.
20. Stephens, W.Z., et al., *The composition of the zebrafish intestinal microbial community varies across development.* ISME J, 2016. **10**(3): p. 644-54.
21. Abayneh, T., D.J. Colquhoun, and H. Sorum, *Edwardsiella piscicida sp. nov., a novel species pathogenic to fish.* J Appl Microbiol, 2013. **114**(3): p. 644-54.
22. Bujan, N., et al., *Genetic studies to re-affiliate Edwardsiella tarda fish isolates to Edwardsiella piscicida and Edwardsiella anguillarum species.* Syst Appl Microbiol, 2018. **41**(1): p. 30-37.
23. Flores, E.M., et al., *The zebrafish as a model for gastrointestinal tract-microbe interactions.* Cell Microbiol, 2020. **22**(3): p. e13152.
24. Alvers, A.L., et al., *Single continuous lumen formation in the zebrafish gut is mediated by smoothened-dependent tissue remodeling.* Development, 2014. **141**(5): p. 1110-9.
25. McGraw, H.F., et al., *Postembryonic neuronal addition in zebrafish dorsal root ganglia is regulated by Notch signaling.* Neural Dev, 2012. **7**: p. 23.
26. Roberts, G.P., et al., *Comparison of Human and Murine Enteroendocrine Cells by Transcriptomic and Peptidomic Profiling.* Diabetes, 2019. **68**(5): p. 1062-1072.
27. Haber, A.L., et al., *A single-cell survey of the small intestinal epithelium.* Nature, 2017. **551**(7680): p. 333-339.
28. Prober, D.A., et al., *Zebrafish TRPA1 channels are required for chemosensation but not for thermosensation or mechanosensory hair cell function.* J Neurosci, 2008. **28**(40): p. 10102-10.
29. Pan, Y.A., et al., *Robo2 determines subtype-specific axonal projections of trigeminal sensory neurons.* Development, 2012. **139**(3): p. 591-600.
30. Meseguer, V., et al., *TRPA1 channels mediate acute neurogenic inflammation and pain produced by bacterial endotoxins.* Nat Commun, 2014. **5**: p. 3125.
31. Yang, Y., et al., *TRPA1-expressing lamina propria mesenchymal cells regulate colonic motility.* JCI Insight, 2019. **4**(9).
32. Holzer, P., *TRP channels in the digestive system.* Curr Pharm Biotechnol, 2011. **12**(1): p. 24-34.
33. Kokel, D., et al., *Photochemical activation of TRPA1 channels in neurons and animals.* Nat Chem Biol, 2013. **9**(4): p. 257-63.
34. Nagel, G., et al., *Channelrhodopsin-2, a directly light-gated cation-selective membrane channel.* Proc Natl Acad Sci U S A, 2003. **100**(24): p. 13940-5.

35. Cocchiaro, J.L. and J.F. Rawls, *Microgavage of zebrafish larvae.* J Vis Exp, 2013(72): p. e4434.
36. Taraviras, S., et al., *Signalling by the RET receptor tyrosine kinase and its role in the development of the mammalian enteric nervous system.* Development, 1999. **126**(12): p. 2785-97.
37. Bondurand, N. and M.H. Sham, *The role of SOX10 during enteric nervous system development.* Dev Biol, 2013. **382**(1): p. 330-43.
38. Pan, H. and M.D. Gershon, *Activation of intrinsic afferent pathways in submucosal ganglia of the guinea pig small intestine.* J Neurosci, 2000. **20**(9): p. 3295-309.
39. Qu, Z.D., et al., *Immunohistochemical analysis of neuron types in the mouse small intestine.* Cell Tissue Res, 2008. **334**(2): p. 147-61.
40. Johnson, C.D., et al., *Deletion of choline acetyltransferase in enteric neurons results in postnatal intestinal dysmotility and dysbiosis.* FASEB J, 2018. **32**(9): p. 4744-4752.
41. Furness, J.B., et al., *The enteric nervous system and gastrointestinal innervation: integrated local and central control.* Adv Exp Med Biol, 2014. **817**: p. 39-71.
42. Bohorquez, D.V., et al., *Neuroepithelial circuit formed by innervation of sensory enteroendocrine cells.* J Clin Invest, 2015. **125**(2): p. 782-6.
43. Bohorquez, D.V., et al., *An enteroendocrine cell-enteric glia connection revealed by 3D electron microscopy.* PLoS One, 2014. **9**(2): p. e89881.
44. Nozawa, K., et al., *TRPA1 regulates gastrointestinal motility through serotonin release from enterochromaffin cells.* Proc Natl Acad Sci U S A, 2009. **106**(9): p. 3408-13.
45. Li, Z., et al., *Essential roles of enteric neuronal serotonin in gastrointestinal motility and the development/survival of enteric dopaminergic neurons.* J Neurosci, 2011. **31**(24): p. 8998-9009.
46. Ulhaq, Z.S. and M. Kishida, *Brain Aromatase Modulates Serotonergic Neuron by Regulating Serotonin Levels in Zebrafish Embryos and Larvae.* Front Endocrinol (Lausanne), 2018. **9**: p. 230.
47. Tornini, V.A., et al., *Live fate-mapping of joint-associated fibroblasts visualizes expansion of cell contributions during zebrafish fin regeneration.* Development, 2017. **144**(16): p. 2889-2895.
48. Gupta, V. and K.D. Poss, *Clonally dominant cardiomyocytes direct heart morphogenesis.* Nature, 2012. **484**(7395): p. 479-84.
49. Foglia, M.J., et al., *Multicolor mapping of the cardiomyocyte proliferation dynamics that construct the atrium.* Development, 2016. **143**(10): p. 1688-96.
50. Randlett, O., et al., *Whole-brain activity mapping onto a zebrafish brain atlas.* Nat Methods, 2015. **12**(11): p. 1039-46.
51. Roager, H.M. and T.R. Licht, *Microbial tryptophan catabolites in health and disease.* Nat Commun, 2018. **9**(1): p. 3294.
52. Macpherson, L.J., et al., *Noxious compounds activate TRPA1 ion channels through covalent modification of cysteines.* Nature, 2007. **445**(7127): p. 541-5.
53. Gehart, H., et al., *Identification of Enteroendocrine Regulators by Real-Time Single-Cell Differentiation Mapping.* Cell, 2019. **176**(5): p. 1158-1173 e16.
54. Gershon, M.D., *5-Hydroxytryptamine (serotonin) in the gastrointestinal tract.* Curr Opin Endocrinol Diabetes Obes, 2013. **20**(1): p. 14-21.
55. Roach, G., et al., *Loss of ascl1a prevents secretory cell differentiation within the zebrafish intestinal epithelium resulting in a loss of distal intestinal motility.* Dev Biol, 2013. **376**(2): p. 171-86.
56. Bautista, D.M., et al., *TRPA1 mediates the inflammatory actions of environmental irritants and proalgesic agents.* Cell, 2006. **124**(6): p. 1269-82.
57. Smith, T., *A Modification of the Method for Determining the Production of Indol by Bacteria.* J Exp Med, 1897. **2**(5): p. 543-7.
58. Darkoh, C., et al., *A rapid and specific method for the detection of indole in complex biological samples.* Appl Environ Microbiol, 2015. **81**(23): p. 8093-7.

59. Lee, J.H., T.K. Wood, and J. Lee, *Roles of indole as an interspecies and interkingdom signaling molecule.* Trends Microbiol, 2015. **23**(11): p. 707-718.
60. Verbrugghe, E., et al., *Growth Regulation in Amphibian Pathogenic Chytrid Fungi by the Quorum Sensing Metabolite Tryptophol.* Front Microbiol, 2018. **9**: p. 3277.
61. Han, Y., et al., *Mutation of tryptophanase gene tnaA in Edwardsiella tarda reduces lipopolysaccharide production, antibiotic resistance and virulence.* Environ Microbiol Rep, 2011. **3**(5): p. 603-12.
62. Venkatesh, M., et al., *Symbiotic bacterial metabolites regulate gastrointestinal barrier function via the xenobiotic sensor PXR and Toll-like receptor 4.* Immunity, 2014. **41**(2): p. 296-310.
63. Zelante, T., et al., *Tryptophan catabolites from microbiota engage aryl hydrocarbon receptor and balance mucosal reactivity via interleukin-22.* Immunity, 2013. **39**(2): p. 372-85.
64. Bhattarai, Y., et al., *Gut Microbiota-Produced Tryptamine Activates an Epithelial G-Protein-Coupled Receptor to Increase Colonic Secretion.* Cell Host Microbe, 2018. **23**(6): p. 775-785 e5.
65. John Haynes, W., et al., *Indole and other aromatic compounds activate the yeast TRPY1 channel.* FEBS Lett, 2008. **582**(10): p. 1514-8.
66. Nassini, R., et al., *The TRPA1 channel in inflammatory and neuropathic pain and migraine.* Rev Physiol Biochem Pharmacol, 2014. **167**: p. 1-43.
67. Gershon, M.D., *Review article: serotonin receptors and transporters -- roles in normal and abnormal gastrointestinal motility.* Aliment Pharmacol Ther, 2004. **20 Suppl 7**: p. 3-14.
68. Nezami, B.G. and S. Srinivasan, *Enteric nervous system in the small intestine: pathophysiology and clinical implications.* Curr Gastroenterol Rep, 2010. **12**(5): p. 358-65.
69. Uyttebroek, L., et al., *Neurochemical coding of enteric neurons in adult and embryonic zebrafish (Danio rerio).* J Comp Neurol, 2010. **518**(21): p. 4419-38.
70. Kunze, W.A. and J.B. Furness, *The enteric nervous system and regulation of intestinal motility.* Annu Rev Physiol, 1999. **61**: p. 117-42.
71. Du, E.J., et al., *TrpA1 Regulates Defecation of Food-Borne Pathogens under the Control of the Duox Pathway.* PLoS Genet, 2016. **12**(1): p. e1005773.
72. Vincent, A.D., et al., *Abnormal absorptive colonic motor activity in germ-free mice is rectified by butyrate, an effect possibly mediated by mucosal serotonin.* Am J Physiol Gastrointest Liver Physiol, 2018. **315**(5): p. G896-G907.
73. Chandrasekharan, B., et al., *Interactions Between Commensal Bacteria and Enteric Neurons, via FPR1 Induction of ROS, Increase Gastrointestinal Motility in Mice.* Gastroenterology, 2019. **157**(1): p. 179-192 e2.
74. Ghoshal, U.C. and K.A. Gwee, *Post-infectious IBS, tropical sprue and small intestinal bacterial overgrowth: the missing link.* Nat Rev Gastroenterol Hepatol, 2017. **14**(7): p. 435-441.
75. Fulling, C., T.G. Dinan, and J.F. Cryan, *Gut Microbe to Brain Signaling: What Happens in Vagus.* Neuron, 2019. **101**(6): p. 998-1002.
76. Breit, S., et al., *Vagus Nerve as Modulator of the Brain-Gut Axis in Psychiatric and Inflammatory Disorders.* Front Psychiatry, 2018. **9**: p. 44.
77. Bonaz, B., T. Bazin, and S. Pellissier, *The Vagus Nerve at the Interface of the Microbiota-Gut-Brain Axis.* Front Neurosci, 2018. **12**: p. 49.
78. Bercik, P., et al., *The anxiolytic effect of Bifidobacterium longum NCC3001 involves vagal pathways for gut-brain communication.* Neurogastroenterol Motil, 2011. **23**(12): p. 1132-9.
79. Bravo, J.A., et al., *Ingestion of Lactobacillus strain regulates emotional behavior and central GABA receptor expression in a mouse via the vagus nerve.* Proc Natl Acad Sci U S A, 2011. **108**(38): p. 16050-5.

80. Grill, H.J. and M.R. Hayes, *The nucleus tractus solitarius: a portal for visceral afferent signal processing, energy status assessment and integration of their combined effects on food intake.* Int J Obes (Lond), 2009. **33 Suppl 1**: p. S11-5.
81. Han, W., et al., *A Neural Circuit for Gut-Induced Reward.* Cell, 2018. **175**(3): p. 665-678 e23.
82. Travagli, R.A., et al., *Brainstem circuits regulating gastric function.* Annu Rev Physiol, 2006. **68**: p. 279-305.
83. Berthoud, H.R., et al., *Brainstem mechanisms integrating gut-derived satiety signals and descending forebrain information in the control of meal size.* Physiol Behav, 2006. **89**(4): p. 517-24.
84. Jaglin, M., et al., *Indole, a Signaling Molecule Produced by the Gut Microbiota, Negatively Impacts Emotional Behaviors in Rats.* Front Neurosci, 2018. **12**: p. 216.
85. Kunst, M., et al., *A Cellular-Resolution Atlas of the Larval Zebrafish Brain.* Neuron, 2019. **103**(1): p. 21-38 e5.
86. Kawakami, K., *Tol2: a versatile gene transfer vector in vertebrates.* Genome Biol, 2007. **8 Suppl 1**: p. S7.
87. Kwan, K.M., et al., *The Tol2kit: a multisite gateway-based construction kit for Tol2 transposon transgenesis constructs.* Dev Dyn, 2007. **236**(11): p. 3088-99.
88. Cronan, M.R., et al., *Macrophage Epithelial Reprogramming Underlies Mycobacterial Granuloma Formation and Promotes Infection.* Immunity, 2016. **45**(4): p. 861-876.
89. Mathias, J.R., et al., *Enhanced cell-specific ablation in zebrafish using a triple mutant of Escherichia coli nitroreductase.* Zebrafish, 2014. **11**(2): p. 85-97.
90. Pham, L.N., et al., *Methods for generating and colonizing gnotobiotic zebrafish.* Nat Protoc, 2008. **3**(12): p. 1862-75.
91. Espenschied, S.T., et al., *Epithelial delamination is protective during pharmaceutical-induced enteropathy.* Proc Natl Acad Sci U S A, 2019. **116**(34): p. 16961-16970.
92. Love, M.I., W. Huber, and S. Anders, *Moderated estimation of fold change and dispersion for RNA-seq data with DESeq2.* Genome Biol, 2014. **15**(12): p. 550.
93. Schindelin, J., et al., *Fiji: an open-source platform for biological-image analysis.* Nat Methods, 2012. **9**(7): p. 676-82.
94. Tseng, Q., et al., *Spatial organization of the extracellular matrix regulates cell-cell junction positioning.* Proc Natl Acad Sci U S A, 2012. **109**(5): p. 1506-11.
95. Knight, R.D., et al., *Ret signalling integrates a craniofacial muscle module during development.* Development, 2011. **138**(10): p. 2015-24.
96. Rolig, A.S., et al., *The enteric nervous system promotes intestinal health by constraining microbiota composition.* PLoS Biol, 2017. **15**(2): p. e2000689.
97. Ganz, J., et al., *Image velocimetry and spectral analysis enable quantitative characterization of larval zebrafish gut motility.* Neurogastroenterol Motil, 2018. **30**(9): p. e13351.
98. Meijering, E., O. Dzyubachyk, and I. Smal, *Methods for cell and particle tracking.* Methods Enzymol, 2012. **504**: p. 183-200.
99. Naumann, E.A., et al., *From Whole-Brain Data to Functional Circuit Models: The Zebrafish Optomotor Response.* Cell, 2016. **167**(4): p. 947-960 e20.
100. Murdoch, C.C., et al., *Intestinal Serum amyloid A suppresses systemic neutrophil activation and bactericidal activity in response to microbiota colonization.* PLoS Pathog, 2019. **15**(3): p. e1007381.
101. Caceres, A.I., et al., *Transient Receptor Potential Cation Channel Subfamily M Member 8 channels mediate the anti-inflammatory effects of eucalyptol.* Br J Pharmacol, 2017. **174**(9): p. 867-879.